Theses and Dissertations | 1. Thesis and Dissertation Collection, all items

1990-09

Numerical study of non-impulsively started flow around a circular cylinder

Fredrickson, Kent Allen

Monterey, California: Naval Postgraduate School

http://hdl.handle.net/10945/34890

AD-A238 051

NAVAL POSTGRADUATE SCHOOL
Monterey, California

THESIS

NUMERICAL STUDY OF NON-IMPULSIVELY
STARTED FLOW
AROUND A CIRCULAR CYLINDER

by

Kent Allen Fredrickson

September, 1990

Thesis Advisor: T. Sarpkaya

Approved for public release; distribution is unlimited.

91-04990

REPORT DOCUMENTATION PAGE

REPORT SECURITY CLASSIFICATION Unclassified		1b RESTRICTIVE MARKINGS			
SECURITY CLASSIFICATION AUTHORITY		3 DISTRIBUTION/AVAILABILITY OF REPORT Approved for public release; distribution is unlimited			
DECLASSIFICATION/DOWNGRADING SCHEDULE					
PERFORMING ORGANIZATION REPORT NUMBER(S)		5 MONITORING ORGANIZATION REPORT NUMBER(S)			
NAME OF PERFORMING ORGANIZATION Naval Postgraduate School	6b OFFICE SYMBOL (If applicable) 39	7a NAME OF MONITORING ORGANIZATION Naval Postgraduate School			
ADDRESS (City, State, and ZIP Code) Monterey, CA 93943-5000		7b ADDRESS (City, State, and ZIP Code) Monterey, CA 93943-5000			
NAME OF FUNDING/SPONSORING ORGANIZATION	8b OFFICE SYMBOL (If applicable)	9 PROCUREMENT INSTRUMENT IDENTIFICATION NUMBER			
ADDRESS (City, State, and ZIP Code)		10 SOURCE OF FUNDING NUMBERS			
		PROGRAM ELEMENT NO	PROJECT NO	TASK NO	WORK UNIT ACCESSION NO

TITLE (Include Security Classification)
NUMERICAL STUDY OF NON-IMPULSIVELY STARTED FLOW AROUND A CIRCULAR CYLINDER

PERSONAL AUTHOR(S)
Fredrickson, Kent Allen

TYPE OF REPORT Master's Thesis	13b TIME COVERED FROM _____ TO _____	14 DATE OF REPORT (Year, Month, Day) September 1990	15 PAGE COUNT 78

SUPPLEMENTARY NOTATION The views expressed in this thesis are those of the author and do not reflect the official policy or position of the Department of Defense or the U.S. Government

COSATI CODES			18 SUBJECT TERMS (Continue on reverse if necessary and identify by block number)
FIELD	GROUP	SUB-GROUP	Hydrodynamics, Numerical Calculations, Wake, Cylinder, Impulsive Flow

ABSTRACT (Continue on reverse if necessary and identify by block number)

e effect of constant acceleration, prior to the establishment of a steady uniform flow, some of the characteristics of the resulting time-dependent flow about a circular linder has been investigated numerically. It is shown that the occurrence of a cal maximum drag is dependent on the parameters characterizing the non-impulsive ture of the ambient flow. However, the onset of the wake asymmetry and the evolution the lift and drag forces during the transient period depend on the characteristics of e numerical perturbation used to initiate the asymmetric vortex shedding. It is ncluded that the numerical methods can predict, to varying degrees of accuracy, the navior of the symmetric state and the quasi-steady-state, but not of the intermediate ate.

DISTRIBUTION/AVAILABILITY OF ABSTRACT ☒ UNCLASSIFIED/UNLIMITED ☐ SAME AS RPT ☐ DTIC USERS	21 ABSTRACT SECURITY CLASSIFICATION Unclassified	
NAME OF RESPONSIBLE INDIVIDUAL ofessor T. Sarpkaya	22b TELEPHONE (Include Area Code) (408) 646-3425	22c OFFICE SYMBOL MESL

FORM 1473, 84 MAR   83 APR edition may be used until exhausted   SECURITY CLASSIFICATION OF THIS PAGE
All other editions are obsolete

Unclassified

Approved for public release; distribution is unlimited.

Numerical Study of Non-Impulsively Started Flow
Around a Circular Cylinder

by

Kent Allen Fredrickson
Lieutenant, United States Navy
B.S., University of Washington, 1984

Submitted in partial fulfillment
of the requirements for the degree of

MASTER OF SCIENCE IN MECHANICAL ENGINEERING

from the

NAVAL POSTGRADUATE SCHOOL
September 1990

Author:

Kent Allen Fredrickson

Approved by:

T. Sarpkaya, Thesis Advisor

Anthony J. Healey, Chairman
Department of Mechanical Engineering

ii

ABSTRACT

The effect of constant acceleration, prior to the establishment of a steady uniform flow, on some of the characteristics of the resulting time-dependent flow about a circular cylinder has been investigated numerically. It is shown that the occurrence of a local maximum drag is dependent on the parameters characterizing the non-impulsive nature of the ambient flow. However, the onset of the wake asymmetry and the evolution of the lift and drag forces during the transient period depend on the characteristics of the numerical perturbation used to initiate the asymmetric vortex shedding. It is concluded that the numerical methods can predict, to varying degrees of accuracy, the behavior of the symmetric state and the quasi-steady-state, but not of the intermediate state.

Accession For	
NTIS GRA&I	☑
DTIC TAB	☐
Unannounced	☐
Justification	
By	
Distribution/	
Availability Codes	
Dist	Avail and/or Special
A-1	

iii

TABLE OF CONTENTS

iv

LIST OF FIGURES

NOMENCLATURE

A_p = Acceleration parameter = $1/(S/R)_v$

A_{pn} = $D^n(d^n U/dt^n)/V^{n+1}$

C_D = Drag coefficient = $2F/\rho DV^2$

C_{DM} = Maximum drag coefficient

C_i = $4F/(\pi \rho D^2 dU/dt)$

C_L = Lift coefficient = $2L/\rho DV^2$

D = Diameter of circular cylinder = $2R$

F = Drag of in-line force per unit length

L = Lift or traverse force per unit length

R = Radius of the circular cylinder

Re = Reynolds number = VD/v

R_{out} = Radius of the outer boundary

S = Displacement of fluid

S/R = Relative displacement of fluid

$(S/R)_m$ = Relative fluid displacement at which C_{DM} occurs

$(S/R)_v$ = Relative displacement of fluid during the acceleration period

$= 0.5(dU/dt)t_v^2/R = V^2/(DdU/dt)$

$= 1/A_p = 0.5(Vt_v/R)$

St = Strouhal number = D/VT

T = Period of vortex shedding

t = Time

t_v = Time at the end of the acceleration period

U   = Time-dependent velocity

V   = Constant velocity at the end of the acceleration period

Δt = Time step

$\Delta \alpha$ = Disturbance oscillation applied to ambient flow, (in Degrees)

$\Delta \Psi$ = Streamfunction perturbation applied to cylinder

$\Delta \xi$ = Computational grid spacing

$\Delta \lambda$ = Plot grid spacing

ACKNOWLEDGEMENTS

The great thing is to get the true picture, whatever the picture is.

Winston Churchill

The author wishes to express his greatest appreciation to Distinquished Professor T. Sarpkaya for his sincere guidance in our efforts to find the *true picture* and for the education in the methods of scientific research which is more than what is learned, but a way of thinking. For his lessons and inspiration, I will always remember and respect Professor Sarpkaya.

The author is grateful to Professor Charles Dalton and Dr. Xuegeng Wang for their permission to use the computer code they have developed in the course of their investigation of oscillating flows about a cylinder.

I also wish to thank my wife, Katharina, for her patience during the long hours.

I. INTRODUCTION

Unsteady flow past bluff bodies has attracted a great deal of attention since a number of problems of practical importance are unsteady. Among the numerous theoretical, numerical, and experimental investigations, *impulsively-started* steady flow about a circular cylinder has occupied a prominent place partly because of its intrinsic interest towards the understanding of the evolution of separation, vortex formation, growth, and partly because it provided the most fundamental case for the comparison and validation of various numerical methods and codes. However, neither *impulsive start* nor *impulsive stop* is physically realizable. The flow must be accelerated from rest to a constant velocity, in a prescribed manner. This fact gives rise to a series of new questions such as:

1. What is the effect of the initial acceleration, prior to the establishment of a steady uniform flow, on the characteristics of the resulting time-dependent flow?

2. Are there critical values of the governing parameters above or below which the flow may be regarded as almost impulsively-started?

3. How does the rate of accumulation of vorticity, as well as its cross-wake transfer, depend on the initial history of the motion?

The purpose of this investigation is to explore some of these questions through the use of a numerical scheme based on finite-difference methods.

II. BACKGROUND STUDIES

There is a large volume of literature which deals with fluctuating forces and associated vortex shedding from bluff bodies subjected to steady ambient flow. The circular cylinder has attracted by far the greatest attention. Numerous computational studies have been performed on flow about circular cylinders in an attempt to predict the Strouhal number in steady ambient flow and the shape and growth of the wake region in impulsively started steady flow. Here, only the more recent and relatively more accurate examples will be cited. Ta Phuoc Loc [Ref. 1] solved the complete unsteady Navier-Stokes equation in vorticity/stream-function form using a combination of second and fourth-order compact finite-difference schemes. He obtained short-time symmetric-wake solutions at Reynolds numbers of 300, 550, and 1,000 and achieved good agreement with flow visualization results for both vortex size and center position. His calculations also showed clearly the small secondary vortices just behind the separation points.

Lecointe and Piquet [Ref. 2] used several compact schemes with the Navier-Stokes vorticity/stream function formulation to solve laminar flows around circular cylinders up to a Reynolds number of 9500. They studied both start-up and unsteady periodic phenomena. The predicted wake-region shape showed good agreement with experimental flow visualizations. Ta Phuoc Loc and Bouard [Ref. 3]

2

performed calculations at Re = 3,000 and 9,500 using a fourth-order finite-difference technique to solve the Poisson equation for the stream function and a second-order technique for the vorticity-transport equation. They found good agreement between their predictions and flow visualization. The calculations were confined, out of necessity, to relatively short times during which the wake became neither asymmetrical nor turbulent. Chamberlain [Ref. 4] used a second-order fast Poisson solver based on FFT methods and found an accurate solution which agreed well with experiment and the previous computations. Rumsey [Ref. 5] used an upwind-biased implicit approximate factorization algorithm to calculate the impulsively-started unsteady flow over a circular cylinder at a Reynolds number 1200 and a Mach number of 0.3. Rumsey's results were in very good agreement with the previous calculations and showed, predictably enough, only a slight compressibility effect.

All numerical calculations using finite-difference, finite-element, or vortex-element methods (see e.g., Sarpkaya and Shoaff [Ref. 6], van der Vegt [Ref. 7], Sarpkaya [Ref. 8], Chang and Chern [Ref. 9]) have assumed an impulsively-started flow. No computational attempt was made to investigate the effect of the initial acceleration, prior to the establishment of a steady uniform flow, on the characteristics of the resulting time-dependent flow.

Several experimental investigations [Refs. 10-12] of impulsively-started flow around circular and rectangular cylinders

have been carried out. Bouard and Coutanceau [Ref. 10] investigated the shape and growth rate of the wake region behind the cylinder for Reynolds number between 40 and 10,000. Sarpkaya [Ref. 11-12] examined the evolution of the wake region and the development of the lift and drag forces with time for cylinders between Reynolds numbers of 15,000 and 120,000. Nagata et al. [Ref. 13] studied the start-up flow at Reynolds number between 250 and 1200, with the majority of the experiments performed at Re = 1200. They gave detailed results for the time-evolution of the vortical region, boundary-layer parameters, and profile shapes at this Reynolds number. Sarpkaya and Kline [Ref. 14] examined the impulsively-started flow about four types of bluff bodies. Sarpkaya and Ihrig [Ref. 15] performed experiments and vortex-element analysis of impulsively-started flow about rectangular prisms and pointed out emphatically that other than numerical experiments, there is no mechanical system which is capable of generating a truly impulsive flow. In fact, efforts to generate i.ipulsive or uniformly-accelerated flow at high Reynolds numbers may be hampered by the generation of compression and rarefaction waves and regions of intense cavitation (in liquids). Because of this reason one or more acceleration parameters such as

$$A_p = D \frac{(\frac{dU}{dt})}{V^2} \tag{1}$$

4

or

$$A_{pn} = D^n \frac{\frac{d^n U}{dt^n}}{V^{n+1}}$$
(2)

will have to be added to the list of the parameters governing the phenomenon in order to account for the initial history of the fluid motion. The other parameters are the Reynolds number Re = VD/ν and the relative displacement of the ambient flow, given by

$$\frac{S}{R} = 0.5 \frac{(\frac{dU}{dt}) t^2}{R} = 0.5 \frac{Vt^2}{(Rt_v)} \quad for \ t \leq t_v$$
(3)

and

$$\frac{S}{R} = 0.5 (V \frac{t_v}{r}) + (t - t_v) \frac{V}{R} \quad for \ t > t_v$$
(4)

where U is the time-dependent velocity in the interval (0<t<t_v), V is the constant velocity arrived at the end of the acceleration period, R is the radius of the cylinder, t is the time, and t_v is the duration of the acceleration period. Introducing the dimensionless parameter defined by

$$\tau = V \frac{t}{R}$$
(5)

5

and

$$\left(\frac{S}{R}\right)_v = \frac{Vt}{(2R)} = \frac{\tau_v}{2} = \frac{1}{A_p} \tag{6}$$

and taking $V = R = 1$, Equations (1) through (4) may be reduced to

$$S = \left(\frac{\tau^2}{2\tau_v}\right) = \frac{\tau^2}{4S_v} \quad for \ t < \tau_v \tag{7}$$

and

$$S = S_v + (\tau - \tau_v) \quad for \ \tau > \tau_v \tag{8}$$

where $\tau_v = 2S_v$.

A systematic numerical variation of the governing parameters for an arbitrary $U(t)$ is extremely difficult. Thus, to make progress one must begin with the simplest possible unsteadiness, namely, with constant dU/dt, so as to be able to incorporate progressively more complex variations of velocity with time.

6

III. NUMERICAL REPRESENTATION

A. INTRODUCTION

The fluid is assumed to be two-dimensional, incompressible and viscous. The governing equations for the solution are the Navier-Stokes equations with the stream function and the vorticity as independent variables. To achieve a higher density of mesh points near the cylinder surface, the computational domain is transformed from the physical plane (polar coordinates) to a rectangular plane. In the rectangular plane, the mesh is maintained at a uniform grid spacing. It is necessary to have more mesh points closer to the cylinder surface because in this region the gradients of both the vorticity and the stream function are the largest.

A third-order in time, second-order in space, three-level predictor-corrector finite-difference scheme is used to solve the vorticity-transport equation. A Fast Poisson Solver based on the High Order Difference approximation with Identity Expansion (HODIE) and the Fast Fourier Transformation (FFT) provided by the IMSL mathematics library is used to solve for the stream function.

B. GOVERNING EQUATIONS IN THE PHYSICAL DOMAIN

Here only a brief description of the computational method is presented. A more in depth description is given by

7

Wang [Ref. 16]. The unsteady Navier-Stokes equations in the polar coordinates, as defined by the vorticity transport equation and the vorticity/stream-function equation are,

$$\partial \frac{\omega}{\partial t} - \frac{1}{r} \left[\frac{\partial}{\partial r} \left(\omega \partial \frac{\psi}{\partial \theta} \right) - \frac{\partial}{\partial \theta} \left(\omega \partial \frac{\psi}{\partial r} \right) \right] = v \nabla^2 \omega \qquad (9)$$

and

$$\nabla^2 \psi = \omega \qquad (10)$$

where

$$\nabla^2 = \frac{\partial^2}{\partial r^2} + \frac{1}{r} \frac{\partial}{\partial r} + \frac{1}{r^2} \frac{\partial^2}{\partial \theta^2} . \qquad (11)$$

ω and Ψ are the vorticity and the stream function, v is the kinematic viscosity, t is the time and, r and Θ are polar coordinates directions (see Figure 1). The velocity components in the r and Θ directions are defined by

$$u = -\frac{1}{r} \frac{\partial \psi}{\partial \omega} \qquad (12)$$

and

$$v = \frac{\partial \psi}{\partial \omega} . \qquad (13)$$

8

The boundary conditions for the physical problem are: (1) no slip and zero normal velocity on the surface of the cylinder

$$\psi = \frac{\partial \psi}{\partial r} = 0, \quad on \ r=R \qquad (14)$$

and; (2) the potential flow at infinity is defined as

$$\psi = U(r - \frac{R}{r}) \sin\theta \qquad (15)$$

and

$$\omega = 0 \qquad at \ r = \infty$$

where U is the external flow and R is the radius of the cylinder.

The ambient flow is prescribed by

$$
\begin{array}{ll}
\frac{S}{R} = 0 & U=0 \\
0 < \frac{S}{R} < (\frac{S}{R})_v & U = (\frac{dU}{dt}) t \\
\frac{S}{R} > (\frac{S}{R})_v & U=1
\end{array}
\qquad (16)
$$

in which S/R is the relative displacement of the fluid and (dU/dt) is the constant acceleration.

C. TRANSFORMATION FROM PHYSICAL TO COMPUTATIONAL DOMAIN

The coordinate transformations required to go from the physical domain to the computational domain are:

$$r = R \exp(a\xi) \quad \text{and} \quad \Theta = a\eta$$

where R is the radius of the cylinder, a is a transformation parameter (see Figure 2). After non-dimensionalizing the vorticity-stream function equations the transformed equations reduce to:

$$g(\xi)\frac{\partial\overline{\omega}}{\partial\tau} - \frac{\partial}{\partial\xi}\left(\frac{\partial\overline{\psi}}{\partial\eta}\overline{\omega}\right) + \frac{\partial}{\partial\eta}\left(\frac{\partial\overline{\omega}}{\partial\xi}\overline{\omega}\right) = \frac{2}{Re}\nabla^2\overline{\omega} \tag{17}$$

and

$$\nabla^2\overline{\psi} = g(\xi)\,\overline{\omega} \tag{18}$$

where

$$\nabla^2 = \frac{\partial^2}{\partial\xi^2} + \frac{\partial^2}{\partial\eta^2} \tag{19}$$

and

$$g(\xi) = a^2\exp(2a\xi). \tag{20}$$

The non-dimensional fluid velocity components in the ξ and η directions are given by

$$\overline{u} = \frac{U}{\sqrt{g(\xi)}} \tag{21}$$

10

and

$$\bar{V} = \frac{V}{\sqrt{g(\xi)}} \tag{22}$$

with U and V defined as

$$U = -\frac{\partial \bar{\psi}}{\partial \eta} \tag{23}$$

and

$$V = \frac{\partial \bar{\psi}}{\partial \xi} \; . \tag{24}$$

The boundary conditions in the computational domain are:

$$\bar{\psi} = \frac{\partial \bar{\psi}}{\partial \xi} = 0 \tag{25}$$

at $\xi = 0$;and

$$\bar{\psi} = 2\bar{U} \sinh(a\xi) \sin(a\eta), \tag{26}$$

and

$$\bar{\omega} = 0 \tag{27}$$

at $\xi = \infty$; and

11

$$\overline{\Psi}(\xi,\eta) = \overline{\Psi}(\xi,\eta + \frac{2\pi}{a}), \tag{28}$$

and

$$\overline{\omega}(\xi,\eta) = \overline{\omega}(\xi,\eta + \frac{2\pi}{a}). \tag{29}$$

The effect of the transformation upon the mesh spacing in the physical is seen in Figure 1. The bar over the non-dimensional quantities will no longer be used for the sake of simplicity. All further quantities should be understood to be non-dimensional.

D. DESCRIPTION OF FINITE DIFFERENCE SCHEME

The finite difference scheme is really a combination of two different schemes as previously described. The use of a central difference scheme to spatially discretize equation (17) leads to

$$g(\xi_{i,j})\frac{\partial\omega_{i,j}}{\partial\tau} = -\frac{U_{i,j+1}\omega_{i,j+1} - U_{i,j-1}\omega_{i,j-1}}{2\delta\xi} - \frac{V_{i+1,j}\omega_{i+1,j} - V_{i-1,j}\omega_{i-1,j}}{2\delta\eta} \tag{30}$$
$$+ \frac{2}{Re}(\frac{\omega_{i,j+1} - 2\omega_{i,j} + \omega_{i,j-1}}{\delta\xi^2} + \frac{\omega_{i+1,j} - 2\omega_{i,j} - \omega_{i-1,j}}{\delta\eta^2}),$$

where i,j represent the ith node in the η direction and the jth node in the ξ direction. The nodal velocities are represented by:

12

$$U_{i,j} = -\frac{\Psi_{i+1,j} - \Psi_{i-1,j}}{2\delta\eta} \qquad (31)$$

and

$$V_{i,j} = \frac{\Psi_{i,j+1} - \Psi_{i,j-1}}{2\delta\xi} . \qquad (32)$$

For further simplification define

$$f_{i,j} = \frac{1}{g(\xi)} \left[-\frac{U_{i,j+1}\omega_{i,j+1} - U_{i,j-1}\omega_{i,j-1}}{2\delta\xi} - \frac{V_{i+1,j}\omega_{i+1,j} - V_{i-1,j}\omega_{i-1,j}}{2\delta\eta} \right. \qquad (33)$$
$$\left. + \frac{2}{Re} \left(\frac{\omega_{i,j+1} - 2\omega_{i,j} + \omega_{i,j-1}}{\delta\xi^2} + \frac{\omega_{i+1,j} - 2\omega_{i,j} - \omega_{i-1,j}}{\delta\eta^2} \right) \right] ,$$

then equation (30) can be simply written as

$$\frac{\partial\omega_{i,j}}{\partial\tau} = f_{i,j} . \qquad (34)$$

Taking the central difference approximation for vorticity and applying a two step, three level, predictor corrector, finite difference scheme with a third order accuracy in time, temporal discretization determines the vorticity in the computational domain. Expanding ω^{n+1} into a Taylor Series and substituting into equation (34) the equation arrived at is

$$\frac{\omega_{i,j}^{n+1} - \omega_{i,j}^n}{\Delta\tau} = f_{i,j}^n + \frac{\partial f_{i,j}^n \Delta\tau}{\partial\tau 2!} + \frac{\partial^2 f_{i,j}^n \Delta\tau^2}{\partial\tau^2 3!} + O(\Delta\tau^3) . \qquad (35)$$

13

The second and third order terms of the right hand side of equation (35) is discretized and becomes

$$\frac{\omega_{i,j}^{n+1}-\omega_{i,j}^{n}}{\Delta\tau}=\frac{5f_{i,j}^{n+1}+8f_{i,j}^{n}-f_{i,j}^{n-1}}{12}+O(\Delta\tau^3) \ . \tag{36}$$

The predictor used is given by the second order Adams-Bashforth method, as shown

$$\omega_{i,j}^{*}=\omega_{i,j}^{n}+\frac{\Delta\tau}{2}(3f_{i,j}^{n}-f_{i,j}^{n-1}) \ , \tag{37}$$

where n is defined as the nth time step and the superscript * indicates the predicted value. The corrector is given by

$$\omega_{i,j}^{n+1}=\omega_{i,j}^{n}+\frac{\Delta\tau}{12}(5f_{i,j}^{*}+8f_{i,j}^{n}-f_{i,j}^{n-1}) \ . \tag{38}$$

The term f^{n-1} is eliminated using equations (37) and (38), leaving the predictor-corrector as,

$$\omega_{i,j}^{n+1}=\frac{1}{6}(\omega_{i,j}^{*}+5\omega_{i,j}^{n})+\frac{5\Delta\tau}{12}(f_{i,j}^{*}-f_{i,j}^{n}) \ . \tag{39}$$

In order to calculate the first time step, the Euler forward method is used to find ω^{*}. The predictor is

$$\omega_{i,j}^{*}=\omega_{i,j}^{1}+\Delta\tau f_{i,j}^{1} , \tag{40}$$

and the corrector is

14

$$\omega_{i,j}^2 = \omega_{i,j}^1 + \frac{\Delta \tau}{2} \left(f_{i,j}^* + f_{i,j}^1 \right) . \tag{41}$$

The non-dimensional time scale is defined by the relative displacement S/R, as noted previously.

E. CALCULATION OF VORTICITY ON THE CYLINDER WALL

Vorticity on the cylinder wall is determined using a Taylor Series expansion of the stream function,

$$\psi(2) = \psi(1) + \left(\frac{\partial \psi}{\partial \xi} \right)_1 \Delta \xi + \left(\frac{\partial^2 \psi}{\partial \xi^2} \right)_1 \frac{\Delta \xi^2}{2!}$$
$$+ \left(\frac{\partial^3 \psi}{\partial \xi^3} \right)_1 \Delta \frac{\xi^3}{3!} + O(\Delta \xi^4) . \tag{42}$$

Equations (18) and (19), and the boundary condition (25) gives

$$\left(\frac{\partial^2 \psi}{\partial \xi^2} \right)_1 = g(1) \omega(1) , \tag{43}$$

and

$$\left(\frac{\partial^3 \psi}{\partial \xi^3} \right)_1 = \left(\frac{\partial (g\omega)}{\partial \xi} \right)_1 = \frac{g(2) \omega(2) - g(1) \omega(1)}{\Delta \xi} + O(\Delta \xi) \tag{44}$$

on the surface of the cylinder. Substituting equations (43) and (44) into equation (42) and using the no slip boundary

15

condition, equation (14) gives

$$\omega(1) = \frac{3\psi(2)}{\Delta\xi^2 g(1)} - \frac{g(2)\,\omega(2)}{2g(1)} + O(\Delta\xi^2) \,. \tag{45}$$

F. CALCULATION OF THE LIFT AND DRAG COEFFICIENTS

The lift and drag coefficients are determined from the contribution of the viscous forces tangential to the flow and the pressure forces acting normal to the surface of the cylinder. The viscous forces are calculated from $\tau_s = \mu\omega$. This relationship gives the total drag force as

$$F_D = -\int_0^{2\pi} p_s \cos(\theta)\,Rd\theta - \int_0^{2\pi} \mu\omega\sin(\omega)\,Rd\theta, \tag{46}$$

and the total lift force as

$$F_L = -\int_0^{2\pi} p_s \sin(\theta)\,Rd\theta + \int_0^{2\pi} \mu\omega\cos(\theta)\,Rd\theta. \tag{47}$$

After dividing both the total drag and total lift equations by $(0.5\ \rho\ U^2\ D)$ and defining

$$\overline{P_s} = \frac{(p_s - p_\infty)}{(\frac{1}{2}\rho U_\infty^2)}, \tag{48}$$

the drag coefficient reduces to

16

$$C_D = -\frac{1}{2}\int_0^{2\pi}\overline{p_s}\cos(\theta)\,d\theta - \frac{2}{Re}\int_0^{2\pi}\overline{\omega}\sin(\theta)\,d\theta, \qquad \textbf{(49)}$$

and the lift coefficient is given

$$C_L = -\frac{1}{2}\int_0^{2\pi}\overline{p_s}\sin(\theta)\,d\theta + \frac{2}{Re}\int_0^{2\pi}\overline{\omega}\cos(\theta)\,d\theta. \qquad \textbf{(50)}$$

The pressure coefficient is determined from the Navier-Stokes equation in terms of dimensionless vorticity. Once integrated with respect to Θ, the equation is

$$\overline{p_s}(\theta) = \overline{p_s}(0) + \frac{4}{Re}\int_0^{2\pi}(\frac{\partial\overline{\omega}}{\partial r})\,|_{r=1}\,d\theta. \qquad \textbf{(51)}$$

Equation (51) is substituted into equations (49) and (50) to determine the numerical scheme for the total lift and drag coefficients,

$$C_D = -\frac{2}{Re}\int_0^{2\pi}\{[\int_0^{\theta}(\frac{\partial\overline{\omega}}{\partial r})\,|_{r=1}\,d\theta]\cos(\theta) + \overline{\omega}\sin(\theta)\}d\theta, \qquad \textbf{(52)}$$

and

$$C_L = -\frac{2}{Re}\int_0^{2\pi}\{[\int_0^{\theta}(\frac{\partial\overline{\omega}}{\partial r})\,|_{r=1}\,d\theta]\sin(\theta) - \overline{\omega}\cos(\theta)\}d\theta. \qquad \textbf{(53)}$$

17

The radial derivative of the vorticity on the surface of the cylinder, used in the lift and drag coefficient calculations, is determined using a discrete pointwise approximation,

$$\left(\frac{\partial \overline{\omega_i}}{\partial \overline{r}}\right)\Big|_{r=1} = \left(\frac{-3\omega_i + 4\omega_{i+1} - \omega_{i+2}}{2\Delta\xi}\right) + O(\Delta\xi^2). \tag{54}$$

IV. DISCUSSION OF RESULTS

A. INTRODUCTION

The numerical experiments were carried out through the use of a VAX-2000 system and the IMSL library. It became quickly evident that the type of calculations performed would require a computer of greater capacity and speed. Nevertheless it was deemed necessary to proceed with the existing system partly to delineate the limitations of the numerical scheme, partly to determine the limits of the disposable parameters, and partly to compare the results of the physical experiments with those of the numerical predictions during the early stages of flow. Typically, a numerical experiment requires about 50,000 times more time than a physical experiment (50,000 sec/1 sec).

The fundamental objective of the calculations was to determine the ranges of flow which can be calculated *accurately*. The extensive literature that exists on the impulsive flow has either concentrated on the initial symmetric state or on the asymmetric late time vortex shedding. However, no systematic attempt was made to determine the upper limit of the early stages, the upper and lower limits of the intermediate indeterminable state, or the lower limit of the quasi-steady-state, in terms of the parameters characterizing the artificial disturbance imposed

on the flow. It has long been recognized that the symmetric state becomes increasingly unstable and the flow sooner or later bifurcates into an asymmetric state. This bifurcation is not an instantaneous event but takes place rather gradually even if the disturbance is imposed suddenly. However, the interesting feature of all the numerical calculations is that the numerical noise and truncation errors are ever present and continue to work on the propensity of the flow to become *naturally* asymmetrical even though the results are far from being natural. Had one been able to devise a sufficiently accurate numerical scheme and a greater-precision computer, one could maintain a longer symmetric state. Evidently, the onset of asymmetry in calculations depends on the characteristics of the physical disturbances. The two types of disturbances used can never be made identical, but they may be made to mimic each other. Thus, it is the hope of the numerical experimenter that the early stages of an impulsively started flow is relatively immune to truncation errors and the imposed, reasonable, artificial perturbation can, therefore, be expected to compare with the physical experiments. However, once the flow becomes asymmetrical the period of transition into a quasi-steady-state depends, to varying degrees of intensity, on the parameters characterizing the numerical disturbance. For small perturbations, the quasi-steady-state may eventually be arrived at smoothly without the lift and drag overshooting first and then reducing to their

20

terminal values. The rather unfortunate aspect of the numerical dilemma is that the quasi-steady-state is not just a function of the characteristics of the perturbation. If it were, one would have conducted a series of numerical experiments, arrived at a fairly stable state, and would have concluded that the flow no longer remembers how it was started and how it ever became asymmetrical. Even though this is the ultimate goal of the numerical experiments, the effects of the unavoidable truncation errors are ubiquitous and continue to influence the entire history of the computed flow. Thus, one may never be able to arrive at an *accurate* solution.

It is in view of the realization of the foregoing facts that the results reported herein dealt with extensive sensitivity calculations to determine the effects of the type and intensity of the perturbations, the grid size, the time increment, and the effect of the outer boundary of the computational domain on the numerical experiments. In view of resources and time limitations noted earlier calculations were confined to standard runs and their variations. For the sake of brevity and for the ease of future reference a run made with:

1. Reynolds number = 1000

2. Disturbance strength = 0.5

3. Sinusoidal disturbance

4. Run time = 40

5. Time step = 0.02

6. Computational grid spacing = 1/64

7. R_{out} = 51R

8. Disturbance interval, S/R = 3-5

9. $(S/R)_v$ = 10

will henceforth be referred to as the standard run.

B. CHARACTERIZATION OF PERTURBATIONS

The problem associated with the assignment of a perturbation is not the making of suitable choices among a limited number of equally sound characterizing parameters, but rather the difficulty of choosing a *reasonable* one from among an infinite set of perturbations and applying it at the *right* time interval. Faced with this problem, previous investigators used many types of artificial disturbances. In fact, there are as many original disturbances as there are original papers. In the present study, two types of disturbances with varying intensities were used. The first, devised by Wang [Ref. 16], was used to perturb the streamfunction on the cylinder from S/R=3 to 5. The shape of the disturbance was a step function. The amplitude of the step $(\Delta\Psi)$ was the only parameter varied while keeping everything fixed, including all other flow features (Re, Δt, R_{out}).

The second type of perturbation was to change the direction of the ambient flow one full sinusoidal cycle in the said S/R range. The amplitude of the sine wave ($\Delta\alpha$) was the only free parameter. It is worth noting that the second type of disturbance is less shock-like and gradually returns the perturbed quantity to its initial state.

Figures 3a and 3b show C_D versus S/R for the first type, step wise disturbance of the streamfunction, with an amplitude of 0.0025. Clearly C_D increases at first, almost impulsively, and then gradually to a maximum value of about 1.25, decreases sharply at the end of the acceleration period ($(S/R)_v=10$), then begins to undergo lift-induced oscillations at $S/R\approx18$. The mean drag continues to increase for a number of reasons, the least of which may be the limited extent of the outer boundary and the reflection there from. The lift reaches a large amplitude after the shedding of the third vortex at an approximate Strouhal number of about 0.23. One must hasten to add that no special accuracy is implied in the stated Strouhal number. It was derived from only a few cycles of oscillations. It must also be clarified that the evolutions of two integrated quantities like lift and drag are not the only means to judge the sensitivity of the predictions to the disturbance characteristics. Nevertheless, they serve to accentuate the said sensitivity better than other quantities such as pressure distribution, vorticity distribution, streamlines or vorticity contours, or velocity and pressure

23

distributions within the flow field. It is because of this reason, that the lift and drag plots will continue to be the only plots referred to during the discussion of the disturbance characteristics.

Figures 4a and 4b show a repeat of the above example with the sole exception that the disturbance strength is doubled. As expected, the stronger the intensity of the disturbance the sooner the inception of the lift and drag oscillations. Otherwise, C_D for S/R<15 remains essentially unchanged.

A more extensive series of numerical experiments were conducted with the second type of disturbance partly because it was more *natural* and more importantly because unlike the first type, this disturbance does not at any time violate the boundary conditions.

Figures 5a-5b through 10a-10b show the drag and lift coefficients for $(S/R)_v=10$ varying only the amplitudes of the sinusoidal disturbance. Figures 5a and 5b are interesting in the sense that the strength of the disturbance is specifically assigned to be zero, and yet the asymmetry is perceptible for S/R>35 (see Figure 5b). As noted earlier, this is due to the inherent truncation errors, and its onset could have been delayed even further had one used higher order or more stable numerical schemes. The remainder of the Figures from 6a to 10b show what one would normally anticipate: the asymmetry sets in sooner, and the oscillations in the drag and lift manifest themselves at S/R values closer to $(S/R)_v$. The

interesting feature of the larger disturbances is that the onset of instability does not start at proportionally smaller S/R values. In fact, the differences between the lift and drag curves for disturbances of $\Delta\alpha = 1.0$ and 2.5 are rather negligible. This may be interpreted as the optimum disturbance to be used to mimic the natural disturbances. However, this is not quite true since the three dimensionality of the disturbances as well as the resulting instabilities encountered in nature may result in significantly different flow characteristics during the transition period. As far as the calculations to be reported herein, a disturbance amplitude of $\Delta\alpha = 0.5$ was chosen.

C. GRID SIZE, TIME-STEP, AND BOUNDARY EFFECTS

These will be discussed in conjunction with each other because of the simple fact that none can be independently varied without violating either the stability constraints or the reflections from the outer boundary.

Figures 11a through 11d show the drag and lift coefficients, and the pressure and vorticity distributions as obtained from a standard run with the exception of the run time equal to 120 and R_{out} equal to 150R. The outer boundary was extended to examine the long term effect of the disturbances on the quasi-steady-state region of the flow. This required the use of a large run time and, in turn, the need to minimize the reflections from the outer boundary.

25

This way, it was possible to carry out the calculations to S/R=120. Figure 11a shows that the drag coefficient exhibits relatively large lift-induced fluctuations in the region of S/R values from approximately 40 to 60. These fluctuations have twice the period of those of lift, as expected. However, for S/R>60 the drag oscillations revert to the same period as the lift oscillations, and synchronize with the vortices shedding from one side of the cylinder. This tends to show that the vortices shed from the cylinder are larger in strength on one side than those from the other side. This is most likely due to the fact that the grid size at large S/R becomes too coarse and the gradients of the various vorticity terms become increasingly inaccurate. It is the realization of this somewhat anticipated fact that led to the decrease of the grid size.

Normally, it would have been desirable to decrease the grid size and at the same time, maintain the outer boundary at the same distance as it was for the coarser grid. Unfortunately, the speed and size constraints of the computer have precluded the need to maintain the size of the computational domain as large as R_{out}=150R. Instead, for an otherwise standard run, the grid spacing was reduced to 1/128, the time step was reduced to 0.01 (to maintain the stability of the computer code), and R_{out} was reduced to 80R. The results of this calculation are shown in Figures 12a through 12d. For the purposes of comparison the drag and lift

coefficients obtained with the two grids ($\Delta\xi=1/64$, $\Delta t=0.02$ and $\Delta\xi=1/128$, $\Delta t=0.01$) are shown in Figures 13a and 13b. Clearly for S/R<10, the results are indistinguishable. For larger values of S/R, there are some differences which do not continue to increase, indicating that both calculations are understandably different and relatively stable at least for S/R<60. Also shown in these figures are the results of a run with a grid size of 1/128 and $\Delta t=0.005$. Surprisingly enough, the two runs with the grid size 1/128 and $\Delta t=0.01$ and $\Delta t=0.005$ are virtually identical and shows that Δt is optimum and the results are dictated by the grid size, as expected.

In summary, the analysis of the sensitivity of the calculations to the variation of the disposable parameters has shown that a standard run is capable of producing sufficiently stable results for S/R<40 with an outer boundary of $R_{out}=51R$. In the section to follow the results obtained with the numerical model will be compared with selected experimental results, obtained at much higher Reynolds numbers (40,000 to 60,000).

D. SOME EXPERIMENTAL RESULTS

Sarpkaya [Ref. 17] investigated experimentally the effect of constant acceleration prior to the establishment of a steady uniform flow on some of the characteristics of the resulting time-dependent flow about a circular cylinder. It was shown that the occurrence of a local maximum drag, the

onset of wake asymmetry, and the evolution of the transverse force are dependent on the parameters characterizing the non-impulsive nature of the ambient flow. The experiments were conducted in a vertical water tunnel at Reynolds numbers considerably larger than those which could possibly be predicted numerically without using a turbulence closure model. Even for the flow with a Reynolds number of 1000 the vortices become turbulent. It is for this reason that the majority of the previous calculations were confined to Reynolds numbers in the order of 100. There are a number of other fundamental differences between the experiments and the numerical model. In computations the flow is strictly laminar and two dimensional. The cylinders in nature have ends. The three dimensionality of the flow induced partly by the instability of the vortices and partly by the cylinder ends may cause differences of varying degrees even if the experiments were performed at Reynolds number corresponding to the calculations.

Figures 14a through 14b for $(S/R)_v=1$, Figs 15a through 15b for $(S/R)_v=5$, and Figures 16a through 16b for $(S/R)_v=10$ show respectively the drag coefficient with and without the use of a numerical perturbation. A careful perusal of the corresponding figures show that for the standard disturbance used, the numerical results do not differ from each other. As noted earlier, the effect of the disturbance exhibits itself for $S/R<40$. The reason for the selection of the S/R range

28

from 0 through 15 was to confine the comparison with experiments through a region relatively unaffected by the parameters characterizing the initial disturbances. Even though this statement is verified within the scope of the numerical calculations, it may not be correct for the physical experiments. Since, strictly speaking, there is no impulsive flow (numerical or experimental) a relatively large acceleration over a prescribed time period will have to be imposed onto the flow about a large enough cylinder to achieve a large enough terminal Reynolds number yielding accurately measurable lift and drag forces. Among the numerous obstacles to these objectives, one particularly stands out: vibrations. Thus, the very early stages of the flow (the first 0.1 or 0.2 seconds) is accompanied not by a constant acceleration but by an acceleration, with a finite rate of change, superimposed on vibrations of high frequency. Thus, comparing the results with experiments one must bear in mind that the Reynolds numbers are not identical and the numerical and experimental flows are not created in the same manner.

Figures 17 through 19 show plots of the numerical and experimental drag coefficients on the same graph for $(S/R)_\tau = 1$, $(S/R)_\tau = 5$, and $(S/R)_\tau = 10$. The experimental results presented were obtained by Sarpkaya [Ref. 17]. It must be emphasized that the discussion refers to the plots shown in the same graph not to their *comparison*.

For $(S/R)_v=1$ the experimental data exhibits a drag overshoot at $S/R \approx 4$ and then the drag decreases gradually to its steady-state value, commonly accepted in the literature. It is important to note that the flow is still nearly symmetrical below $S/R \approx 7$, the drag overshoot is not merely due to the symmetry of the vortices or the accumulation of vorticity in the symmetric vortices. Leaving aside a comparison of their magnitudes, but concentrating on the physics of the evolution of the drag coefficient in Figure 17, one realizes that as the vortices grow symmetrically and as the vorticity accumulates the drag increases to a maximum. Then, the elongation of the vortices the downstream motion of the center of vorticity, plus some mutual annihilation of oppositely-signed vorticity along the axis of symmetry lead to the decrease of the drag coefficient. Thus, it is clear that the drag overshoot has nothing to do with the onset of asymmetry. It depends on only when a symmetric pair of vortices will acquire optimum vorticity at an optimum distance. Since in the experiments, these depend on the initial conditions of imposed acceleration it is not surprising that the measured and predicted drag overshoots do not occur at the same S/R.

Figures 18 through 19 show the effect of the imposed acceleration with greater clarity primarily because of the duration of the acceleration and the relatively smaller amplitude of the initial vibrations. In both figures, the

30

experimental values of the drag coefficient are somewhat smaller for S/R values smaller than $(S/R)_v$. This is explainable in terms of the nature of the acceleration and its time rate of change. For S/R values larger than $(S/R)_v$, the measured values are larger than those calculated. Without attaching undue significance, one may note in passing that C_D (steady) equal to 1.2 for Reynolds number of 10,000 to 100,000 and C_D (steady) equal to 1.0 for a Reynolds numbers of 1000 [Ref. 18]. As far as the rise period of the drag is concerned, calculations contemplated in the near fu...ue will use the instantaneous imposed acceleration as input into the numerical code rather than a constant acceleration, averaged so as to arrive at the same $(S/R)_v$ values.

E. STREAMLINES AND VORTICITY CONTOURS

To provide visual descriptions of the evolution of the velocity and vorticity fields a number of plots with varying degree of close-ups were made. Figure 20 shows for a standard run, but with no disturbance, the symmetric vortex pattern at S/R=5, Figures 21a through 21c show at S/R=15 the streamlines, determined at various grid spacings $(\Delta\lambda)$ about symmetrically evolving vortices. Figure 21c is of some importance in the sense that it shows two phenomenon. The first is physical and related to the so called α phenomena near the downstream shoulders of the cylinder. The other is purely numerical and shows the instability that evolves in the interpolation scheme

31

in a fine grid (here plot grid spacing is 1/160). The said instability has nothing to do with the flow instability but may eventually lead to sufficiently large asymmetries to cause vortex shedding as S/R>40 (see Figure 5b).

Figures 22a and 22b show the streamlines and vorticity contours at S/R=40 for a standard run but without artificial disturbances. There is an almost imperceptibly small asymmetry (see 8 and 10 O'clock positions) as anticipated on the basis of Fig. 5b. Figures 23a and 23b show again at S/R=40 the vortex shedding due to the imposed sinusoidal perturbation with an amplitude of $\Delta\alpha = 0.1$. A superposition of the streamlines (see Figure 23a) and the vorticity lines (see Figure 23b) shows that the center of vorticity is not at the apparent vortex center, a fact which has been known for a long time. This is entirely due to the time dependent nature of the wake. Figures 24a and 24b show the streamlines and vorticity lines at again S/R=40 for a larger sinusoidal disturbance ($\Delta\alpha$ = 0.5). The position of the separation points are not easily identifiable in the foregoing figures because of the crowding of the streamlines near the shoulder of the cylinder. It would be preferable to plot the instantaneous velocity profiles along radial lines to delineate the position of the excursion of the separation points.

Finally, Figures 25a through 25d show the streamlines, the vorticity contours, the pressure distribution, and the vorticity distribution at S/R=40 for a standard run, but using

32

the first type of numerical perturbation with a step amplitude of $\Delta\Psi = 0.005$. The first two plots are similar to, but not directly comparable, with those shown in Figures 24a and 24b. The reason for this is obviously the non-unique nature of the flow and its strong dependence on the characteristics of the perturbation imposed. This is particularly true for large S/R values shown in these figures. The asymmetric nature of the pressure and vorticity is a consequence of the asymmetric vortex development. The lowest pressure occurring at about 80 degrees from the stagnation point is comparable with those calculated by others.

V. CONCLUSIONS

The investigation reported here warranted the following conclusions:

1. Even the higher order finite difference formulations of the governing equations can be solved for only relatively small Reynolds numbers. This is partly due to stability and computer constraints, and in part due to the difficulty of specifying appropriate perturbations forcing the flow to bifurcate into an asymmetric quasi-steady-state.

2. The imposition of various states of uniform acceleration leads to results which have not been previously noted by others. Namely, drag rises to a finite value due to the added mass effect as soon as the acceleration is imposed, then remains fairly constant for a relative displacement less than about two and continues to rise to the end of the acceleration period or until the drag overshoot occurs, depending on whichever comes first.

3. For almost impulsively-started flows the drag overshoot occurs near $S/R=4$. For $(S/R)_v>5$, this overshoot is obsured by the effect of acceleration and continues to increase the drag to values larger than the drag overshoot at $(S/R)_v=4$.

4. The early stages of the flow, i.e. $S/R<15$ can be calculated within the limits of the accuracy of the computational scheme. The results are essentially independent of the characteristics of the perturbation even if they were imposed at the start of the motion.

5. The experimentally observed drag overshoot for almost-impulsively started flow occurs in the range $4<S/R<5$, depending on the noise imposed on the flow at the early stages of the motion.

6. There is a range of S/R values, for both impulsively and non-impulsively started flows, which is not amenable to correct numerical simulation. Because this region depends on the parameters characterizing the perturbations which are unknown and unknowable in physical experiments.

34

7. There is a third region of the flow in which the transient state evolves into a quasi-steady-state. It is assumed, for all intents and purposes that the flow does not remember how it arrived at the quasi-steady-state. It is tacitly assumed that the final state does not depend on the disturbances even though the nonlinear coupling of the disturbances and truncation errors may lead to somewhat different steady states. The existing computer speed and capacity does not allow one to increase the computational domain to arrive at a steady state at the specified Reynolds number.

8. It is a fitting summary that where calculations can be made accurately (S/R<15) experiments are contaminated with noise, where the experiments can be relied upon (S/R>15) calculations cannot be carried out at the corresponding Reynolds numbers, and where the symmetric state bifurcates into an asymmetric state the computations and experiments cannot be compared because the computation depends on the disturbance (15<S/R<40) which cannot be imitated by the numerical perturbations even at the smaller Reynolds numbers. Thus, future researchers must concentrate on conducting numerical experiments at the early and later stages of flow, at Reynolds numbers smaller than 1000 and at carrying out painstakingly difficult force and pressure measurements on cylinders at the same small Reynolds numbers. It is only then that it will be possible to carry out a meaningful comparison between the numerical and physical experiments.
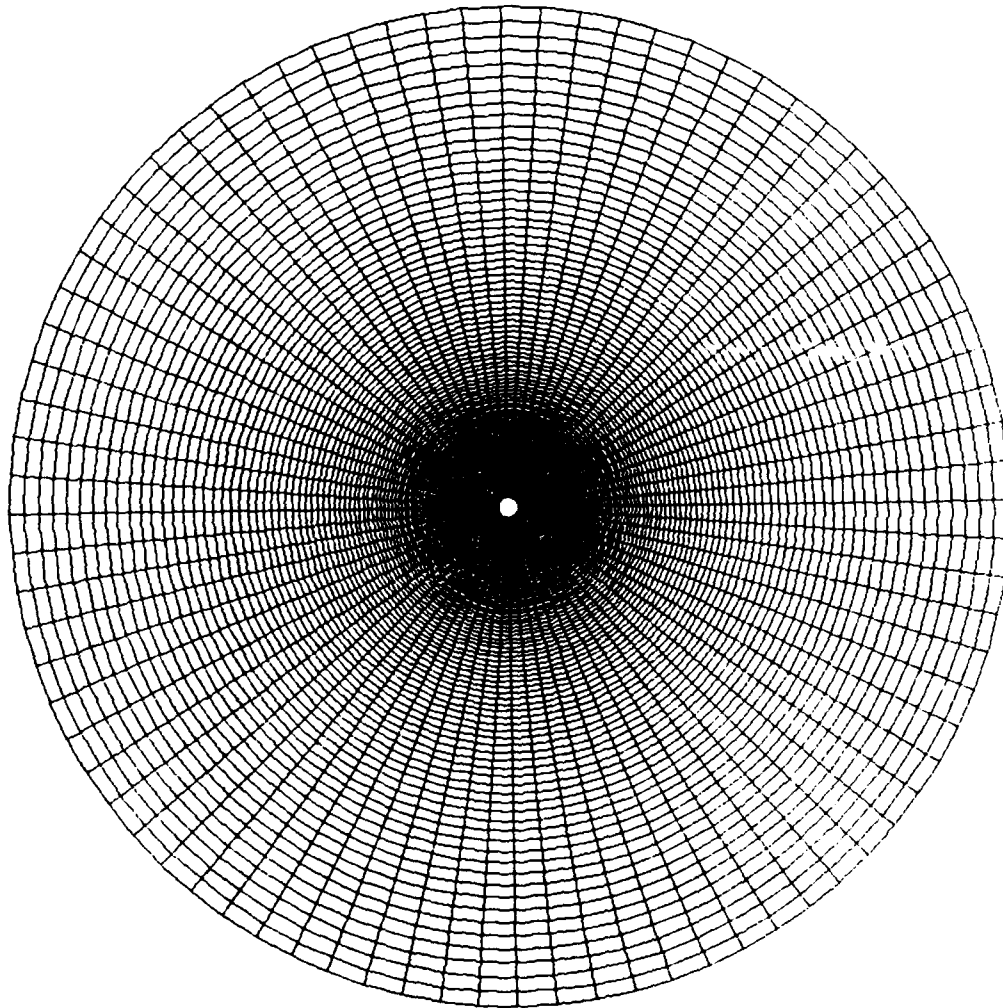
Figure 1. Grid in the Physical Domain
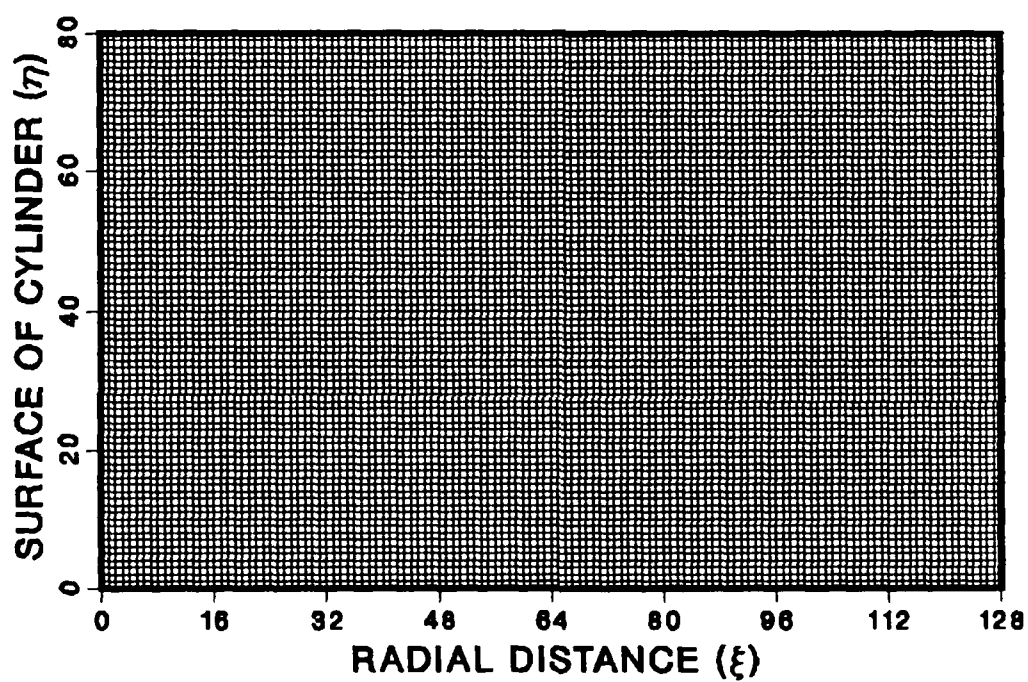
Figure 2. Grid in the Computational Domain
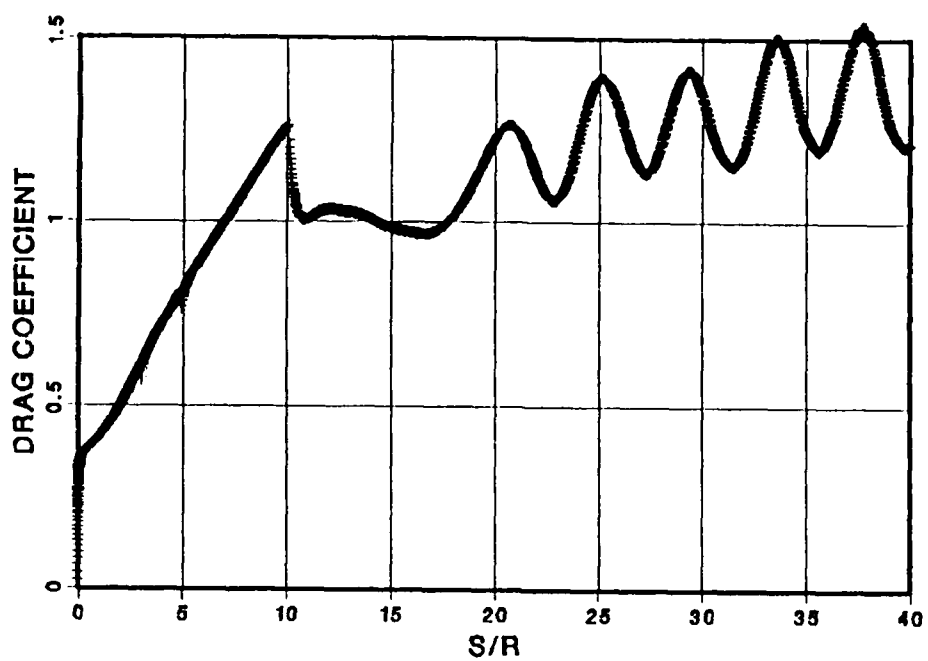
Figure 3a. C_D vs. S/R for $\Delta\Psi$=0.0025
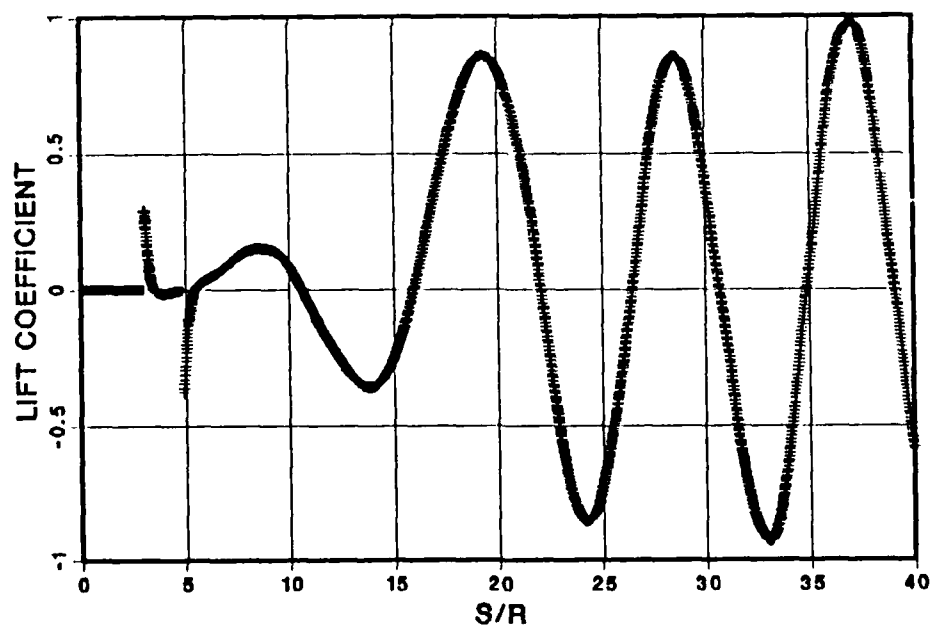
Figure 3b. C_L vs. S/R for $\Delta\Psi$=0.0025

38
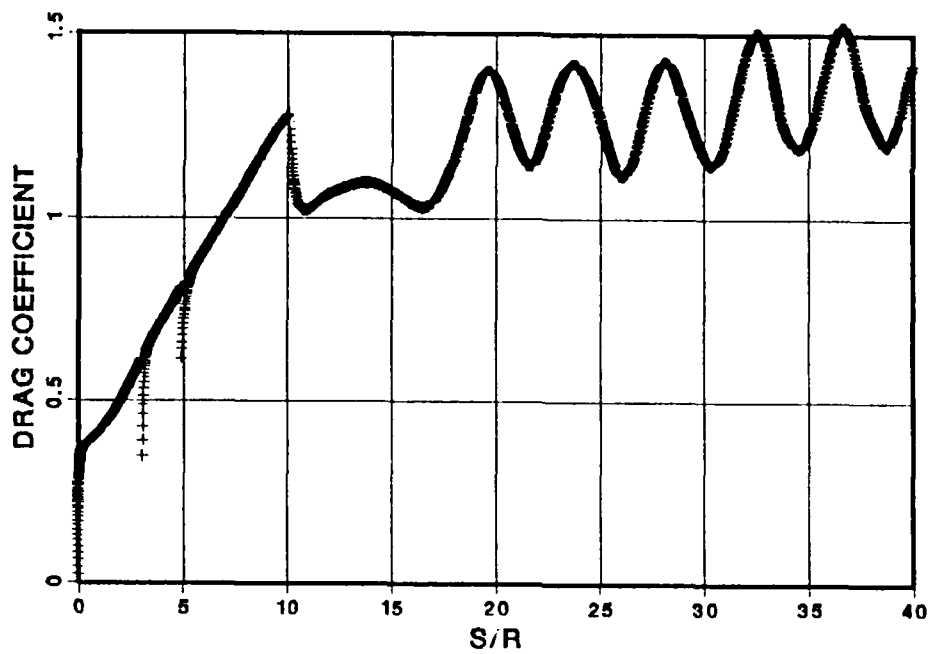
Figure 4a. C_D vs. S/R for $\Delta\Psi=0.005$
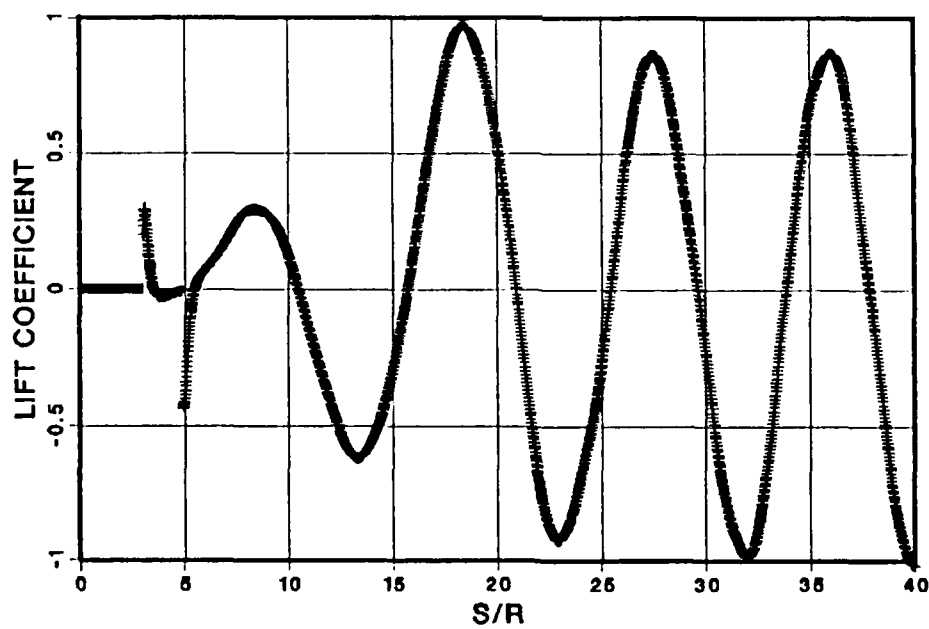
Figure 4b. C_L vs. S/R for $\Delta\Psi=0.005$

39
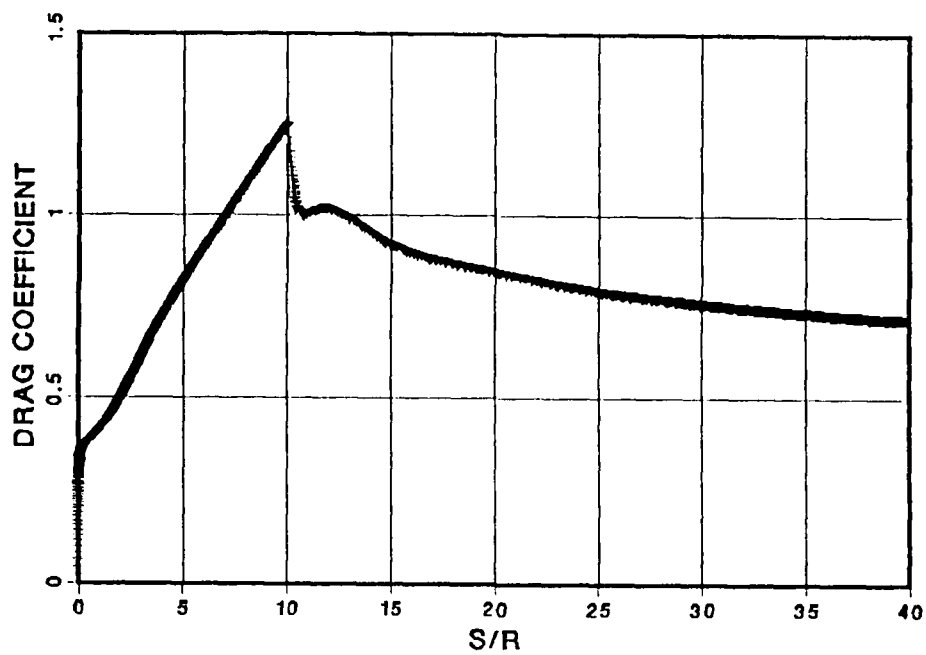
Figure 5a. C_D vs. S/R for $\Delta\alpha = 0.0$
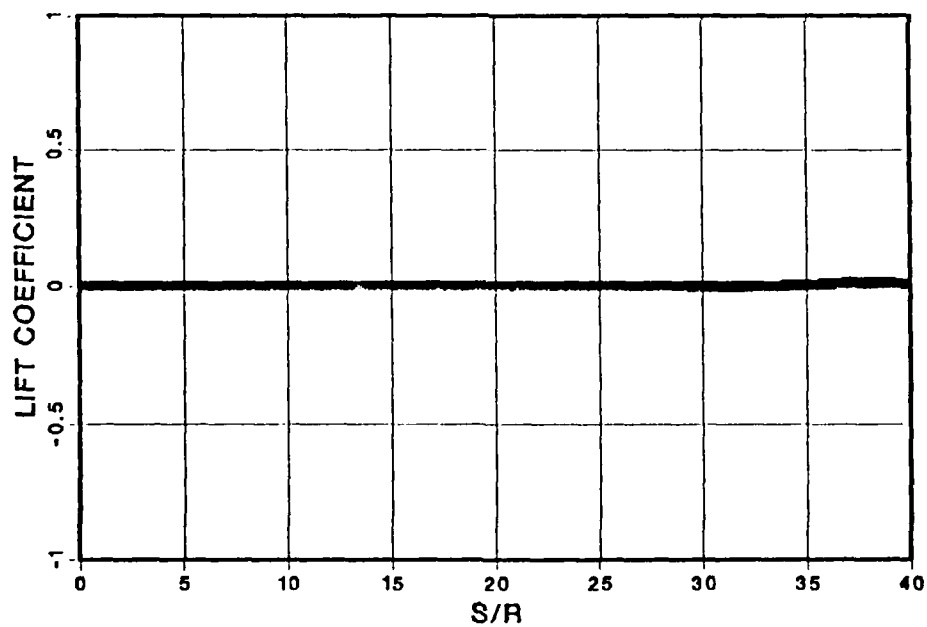
Figure 5b. C_L vs. S/R for $\Delta\alpha = 0.0$

40
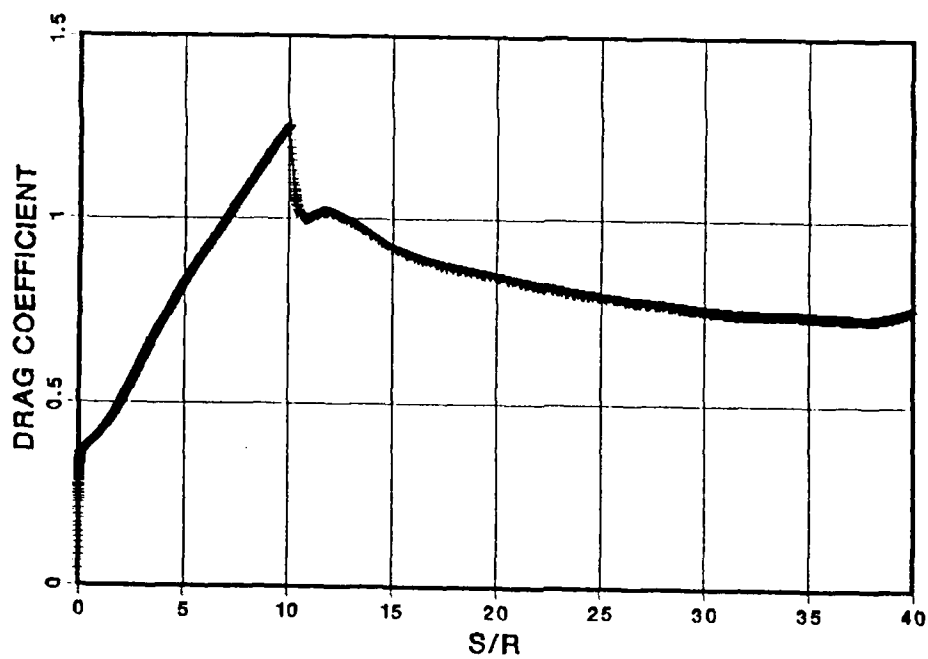
Figure 6a. C_D vs. S/R for $\Delta\alpha$=0.01
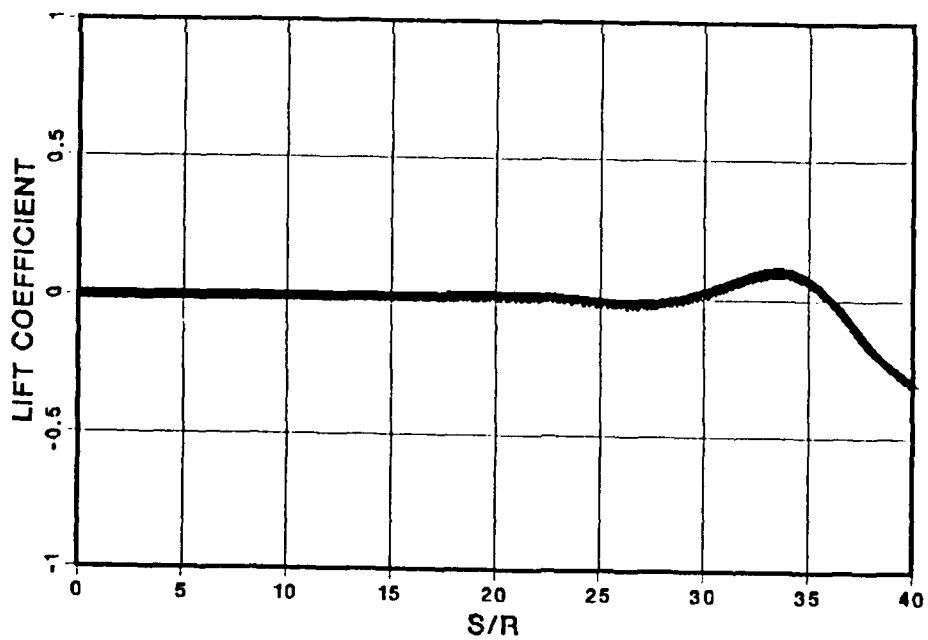
Figure 6b. C_L vs. S/R for $\Delta\alpha$=0.01

41
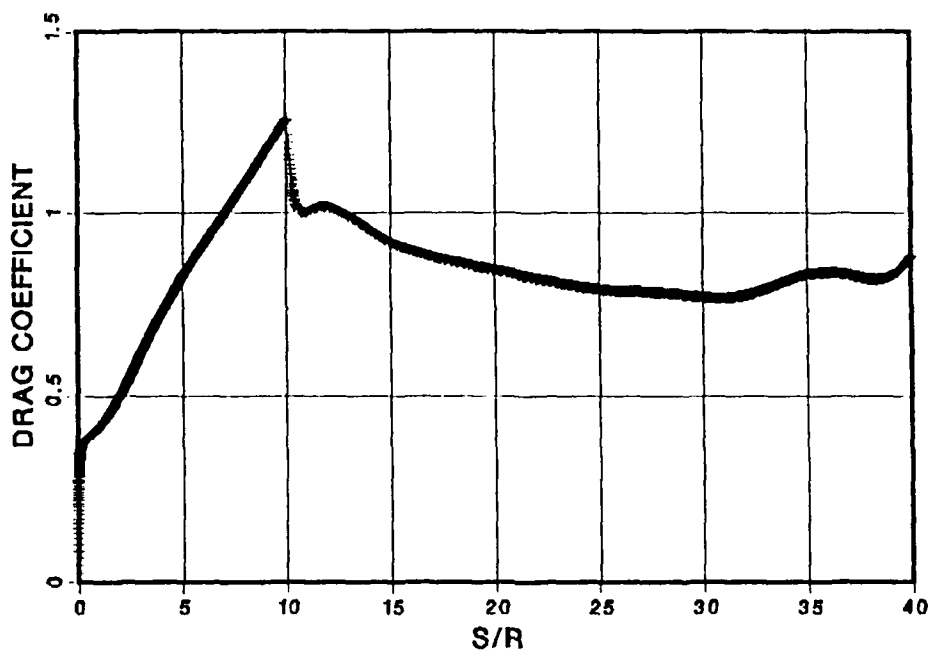
Figure 7a. C_D vs. S/R for $\Delta\alpha$=0.1
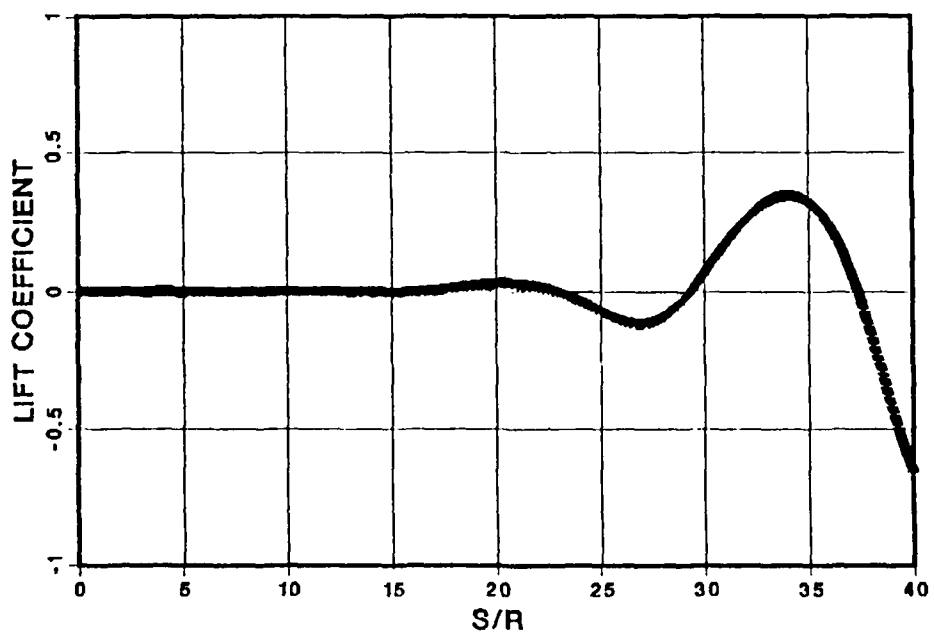
Figure 7b. C_L vs. S/R for $\Delta\alpha$=0.1

42
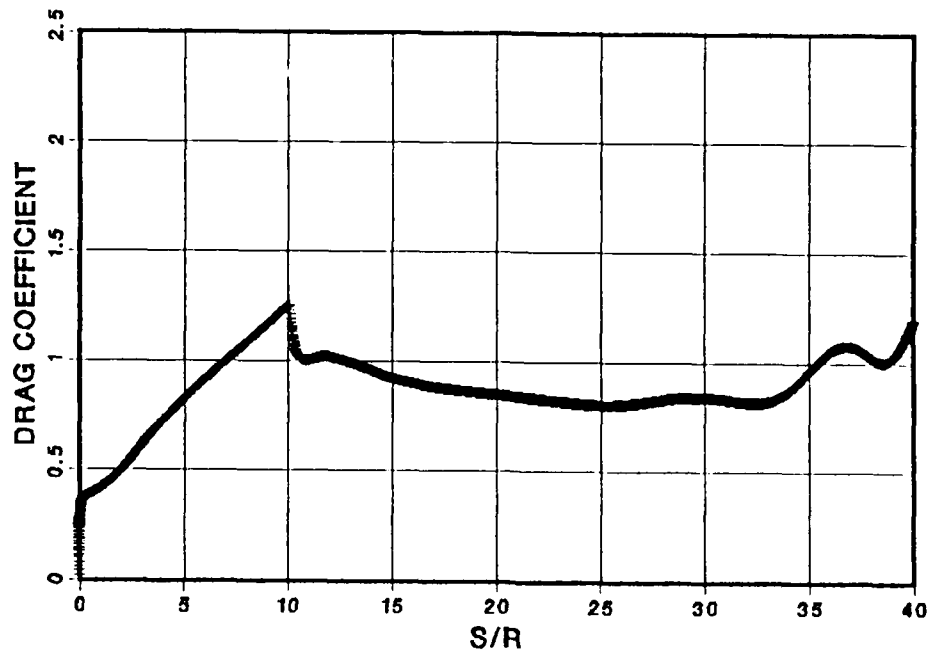
Figure 8a. C_D vs. S/R for $\Delta\alpha=0.5$
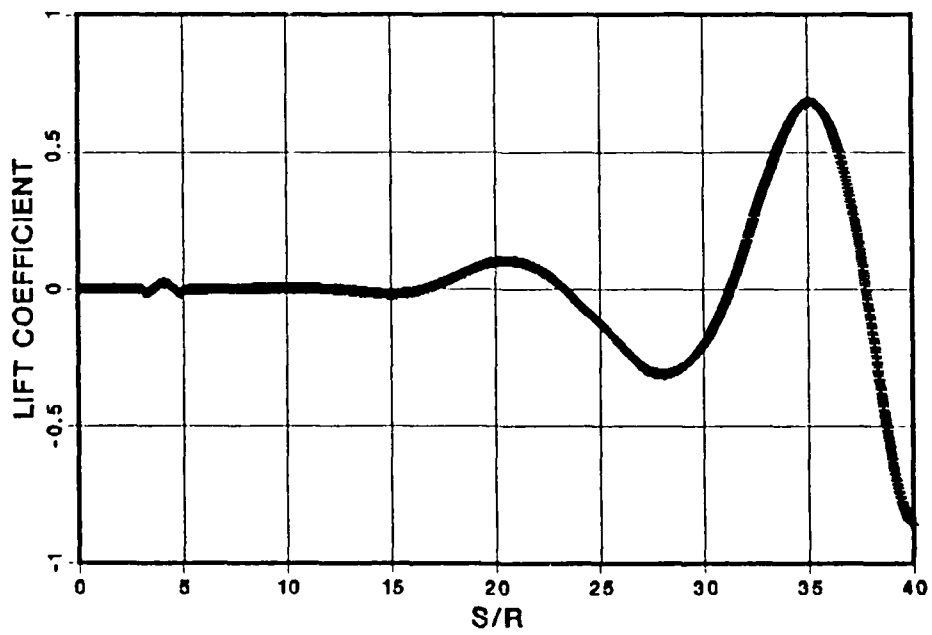
Figure 8b. C_L vs. S/R for $\Delta\alpha=0.5$

43
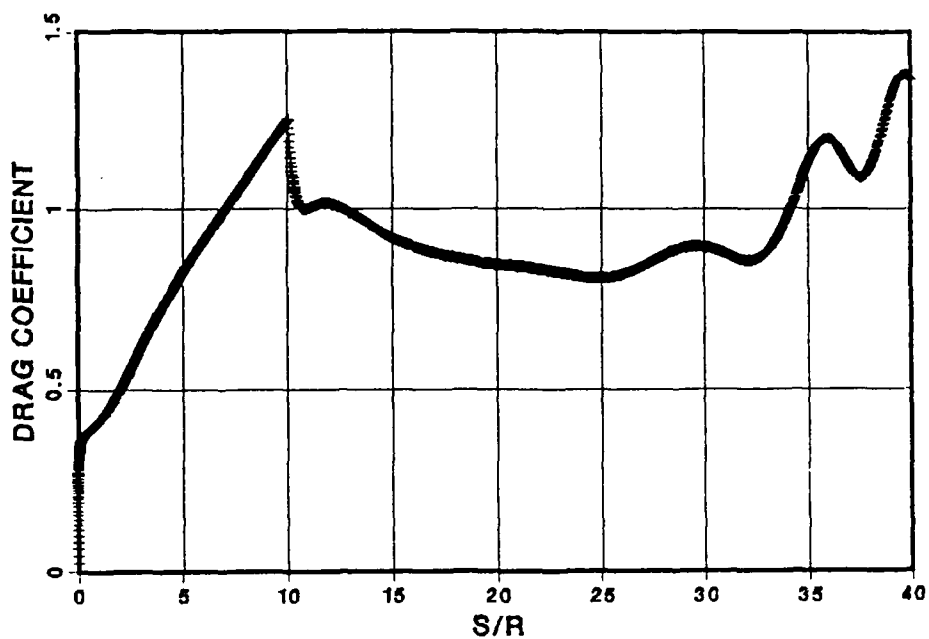
Figure 9a. C_D vs. S/R for $\Delta\alpha$=1.0
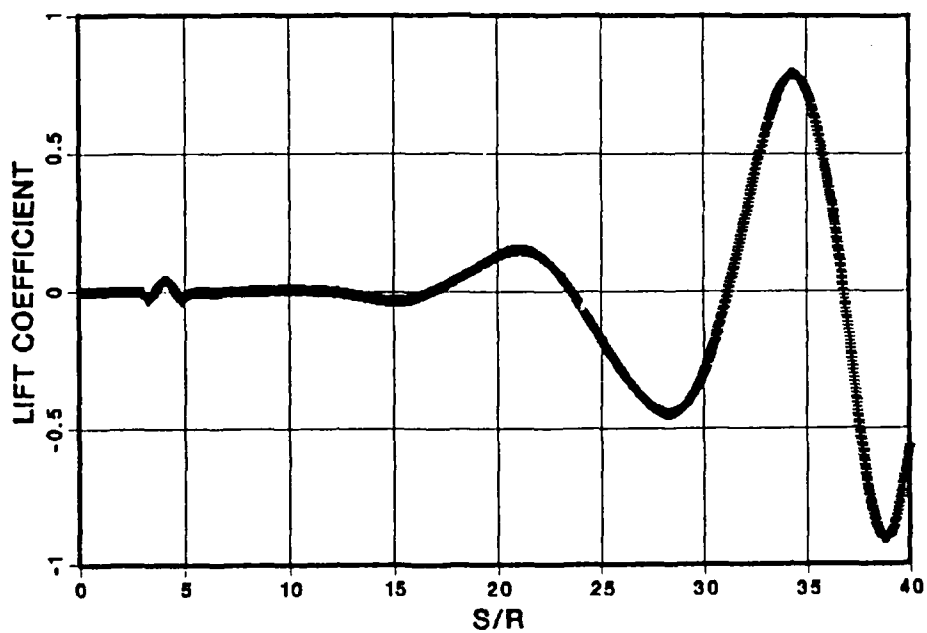
Figure 9b. C_L vs. S/R for $\Delta\alpha$=1.0

44
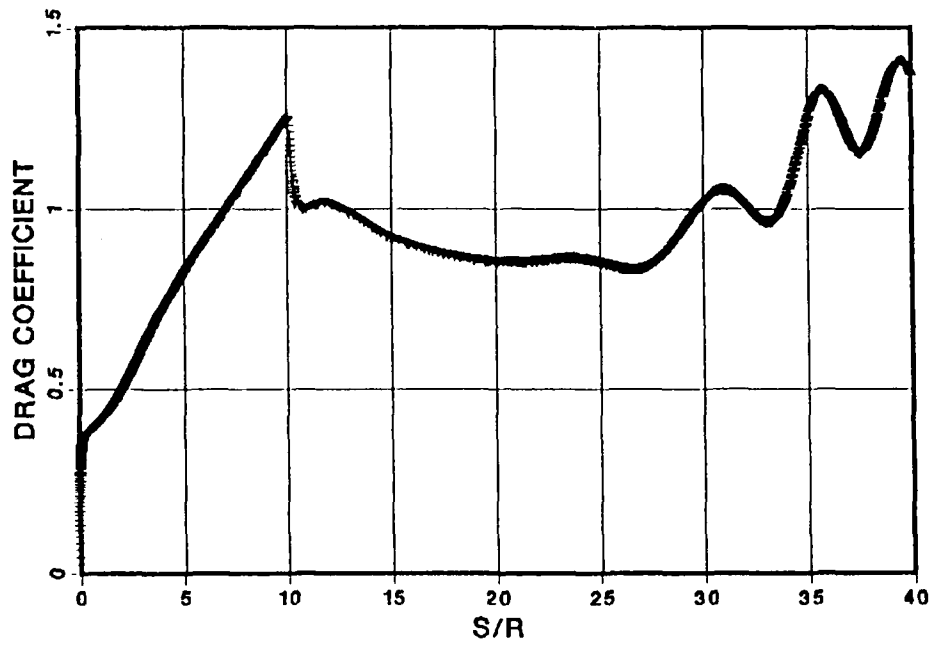
Figure 10a. C_D vs. S/R for $\Delta\alpha=2.5$
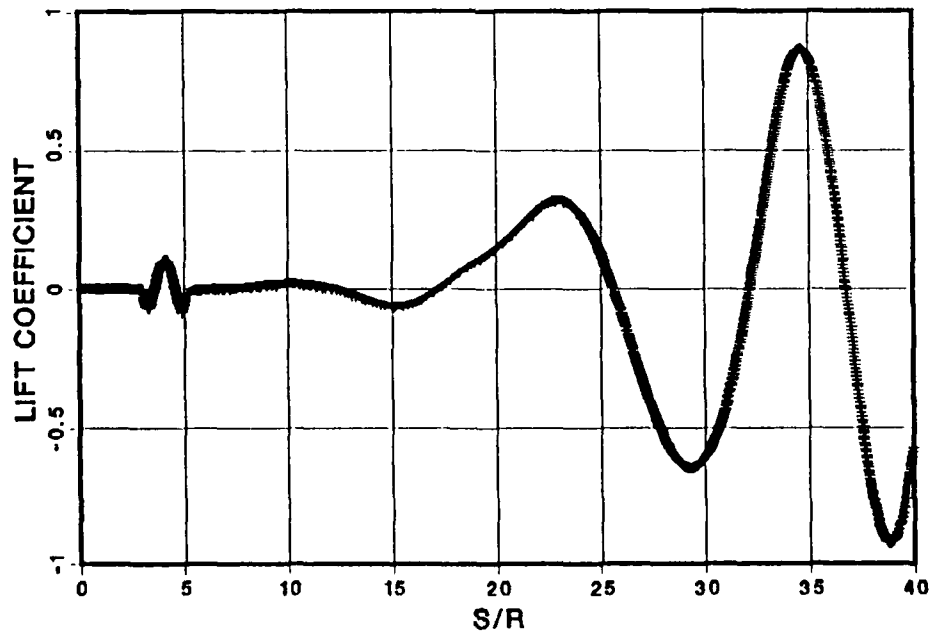
Figure 10b. C_L vs. S/R for $\Delta\alpha=2.5$

45
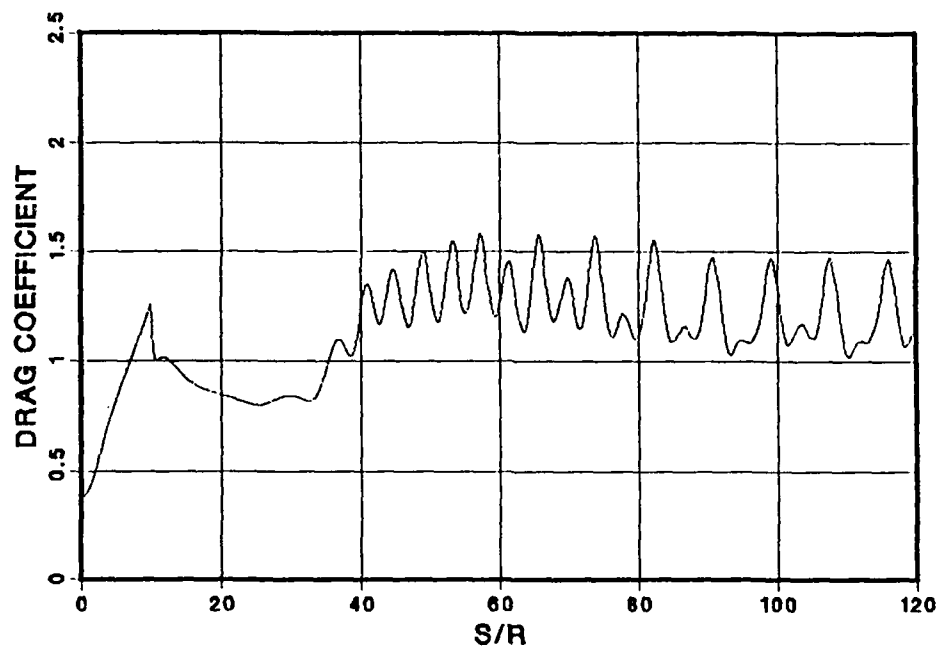
Figure 11a. C_D vs. S/R, $(S/R)_{MAX}=120$, $R_{out}=150R$, and $\Delta\xi=1/64$
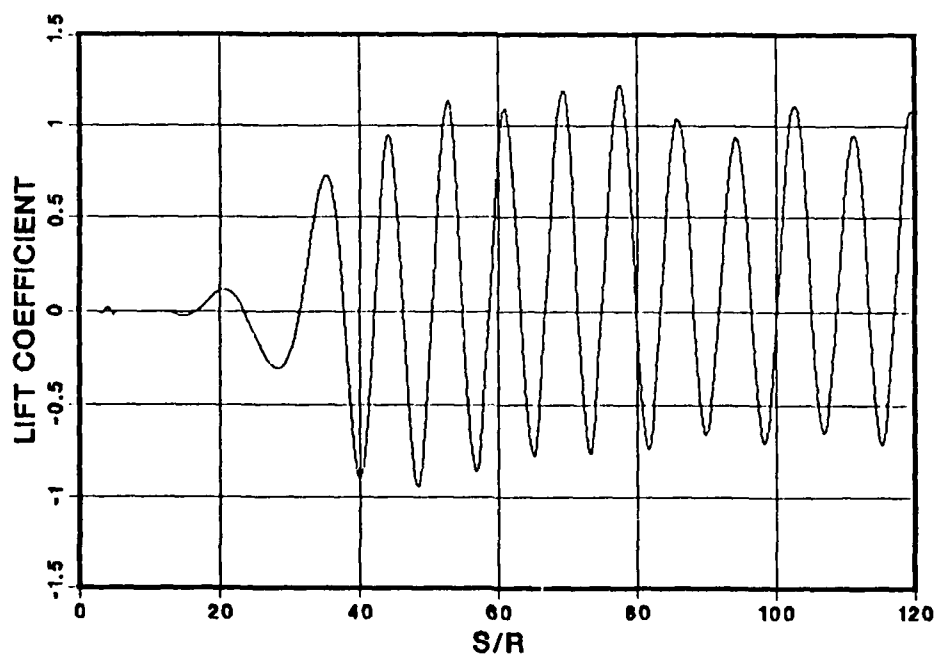
Figure 11b. C_L vs. S/R, $(S/R)_{MAX}=120$, $R_{out}=150R$, and $\Delta\xi=1/64$

46
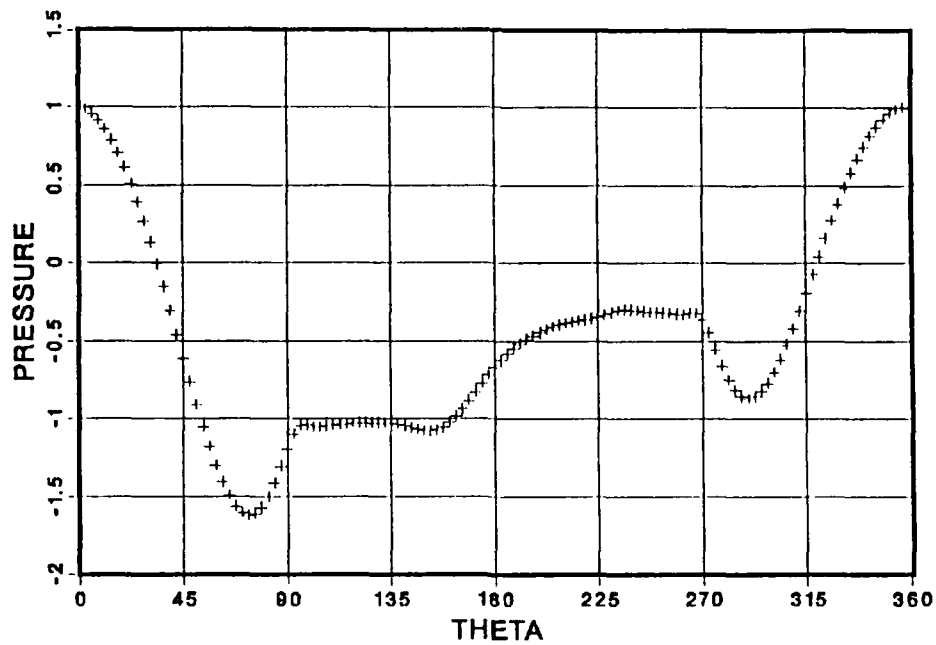
Figure 11c. Pressure Distribution at S/R=120 with $R_{out}=150R$
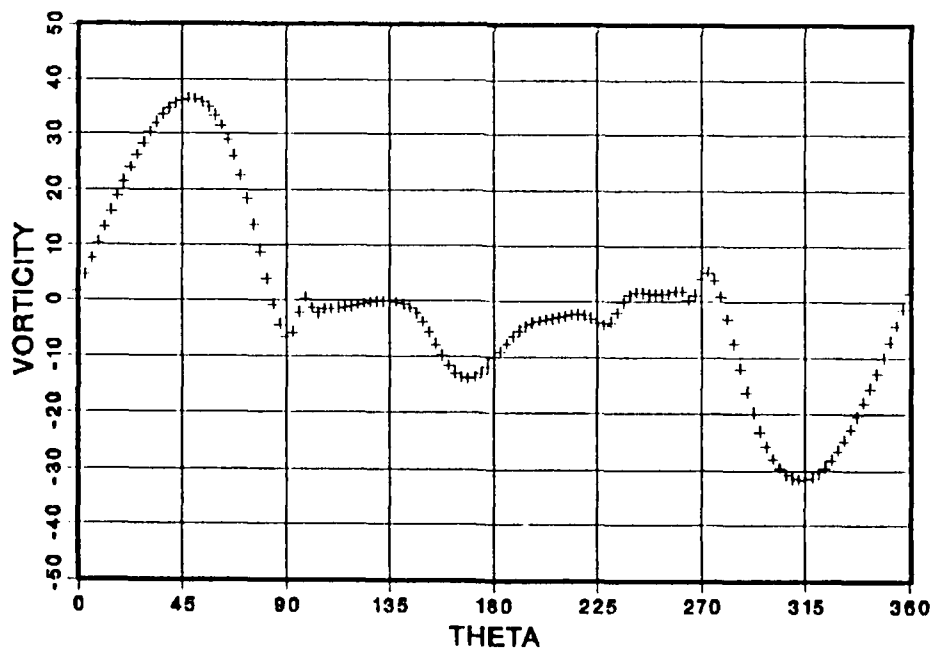
Figure 11d. Vorticity Distribution at S/R=120 with $R_{out}=150R$

47
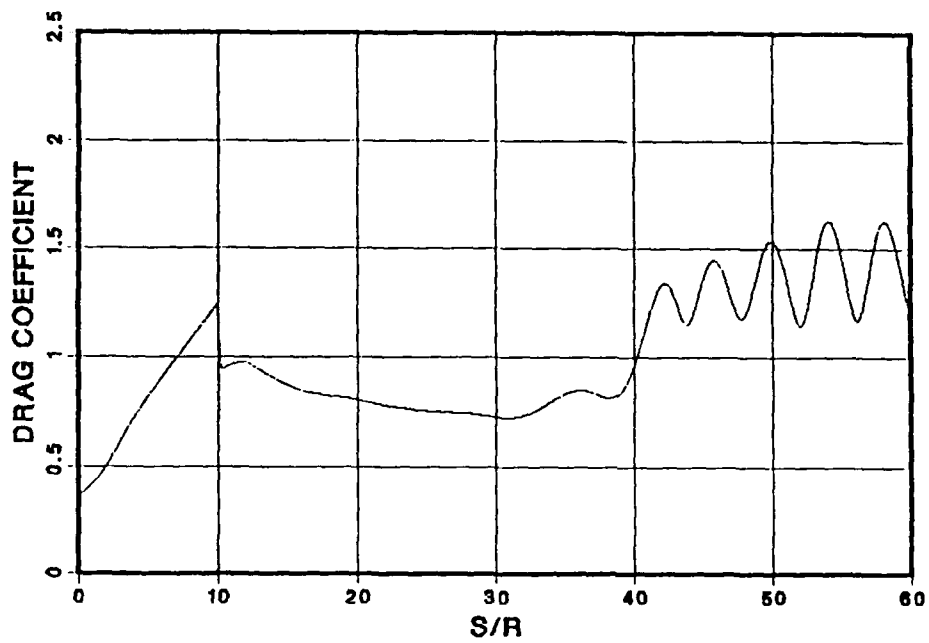
Figure 12a. C_D vs. S/R, $(S/R)_{MAX}=60$, $R_{out}=120$ and $\Delta\xi=1/128$
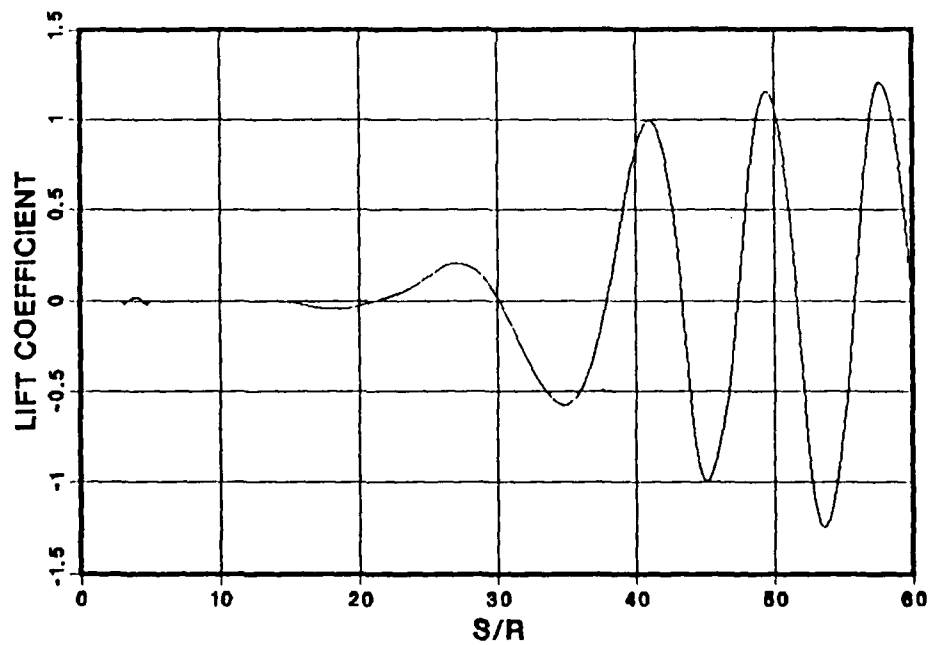
Figure 12b. C_L vs. S/R, $(S/R)_{MAX}=60$, $R_{out}=80R$ with $\Delta\xi=1/128$

48
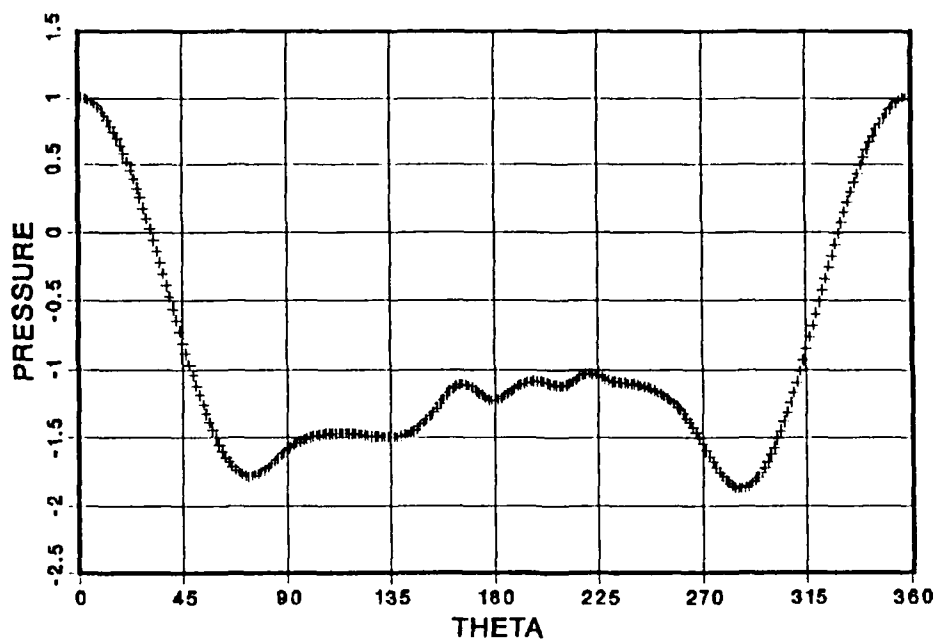
Figure 12c. Pressure Distribution at S/R=60 with R_{out}=80R
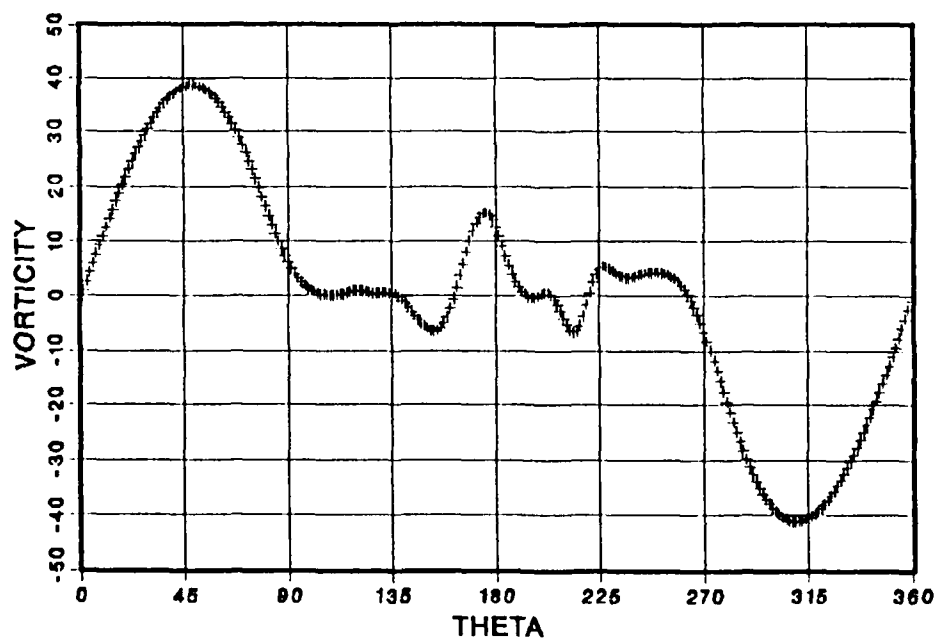
Figure 12d. Vorticity Distribution at S/R=60 with R_{out}=80R

49
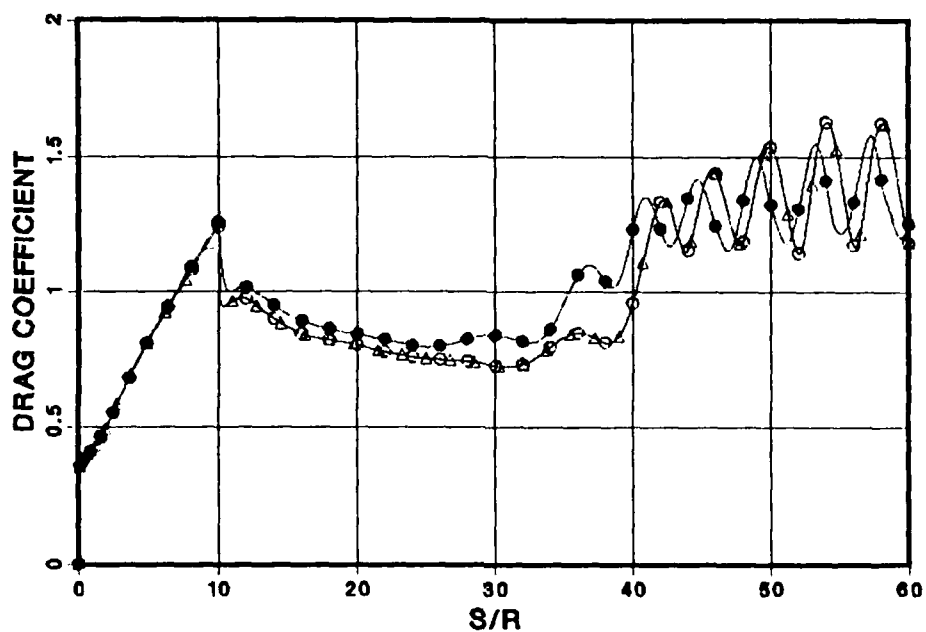
Figure 13a. C_D vs. S/R for $\Delta t=0.02$ and $\Delta\xi=1/64$ (full circle),
$\Delta t=0.01$ and $\Delta\xi=1/128$ (open circle), and $\Delta t=0.005$
and $\Delta\xi=1/128$ (triangle)
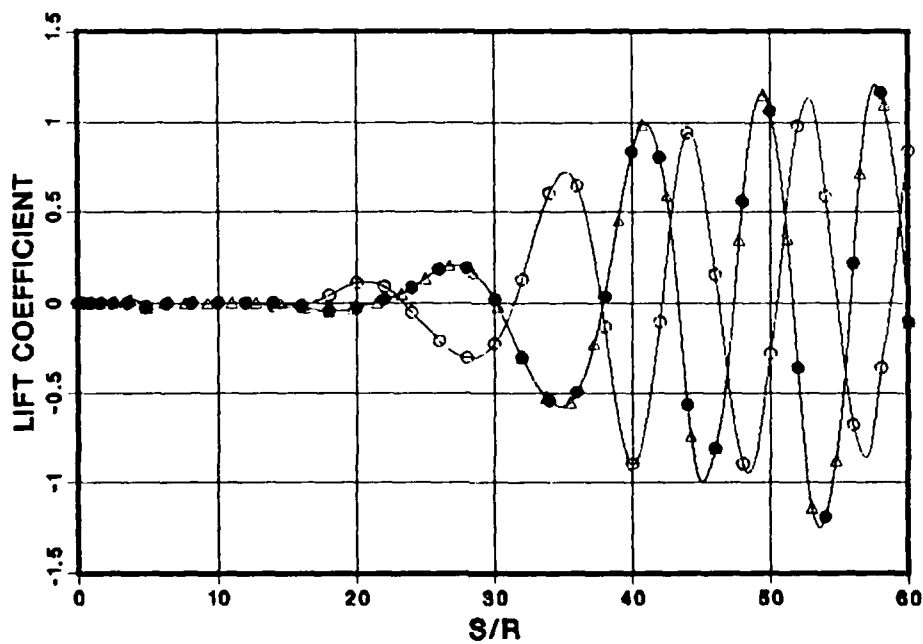
Figure 13b. C_L vs. S/R for $\Delta t=0.02$ and $\Delta\xi=1/64$ (full circle),
$\Delta t=0.01$ and $\Delta\xi=1/128$ (open circle), and
$\Delta t=0.005$ and $\Delta\xi=1/128$ (triangle)

50
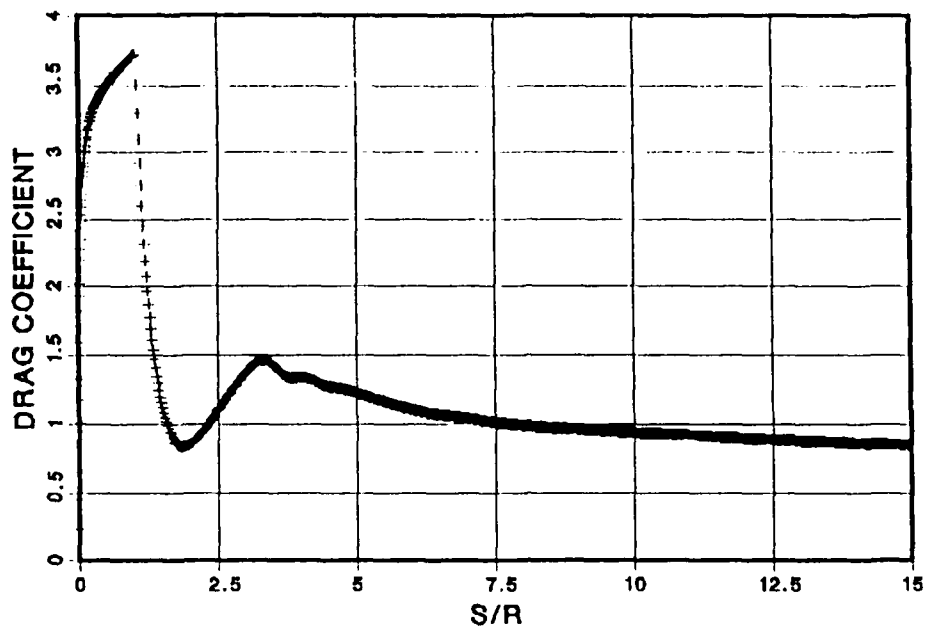
Figure 14a. C_D vs. S/R, $(S/R)_{MAX}=15$ for $(S/R)_v=1$
and No Disturbance
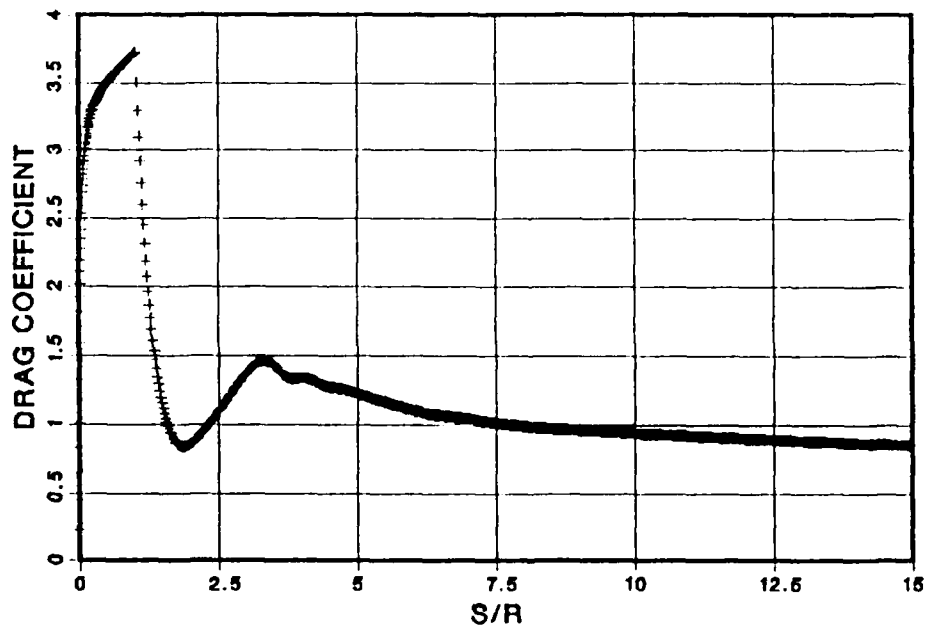
Figure 14b. C_D vs. S/R, $(S/R)_{MAX}=15$ for $(S/R)_v=1$
with $\Delta\alpha=0.5$
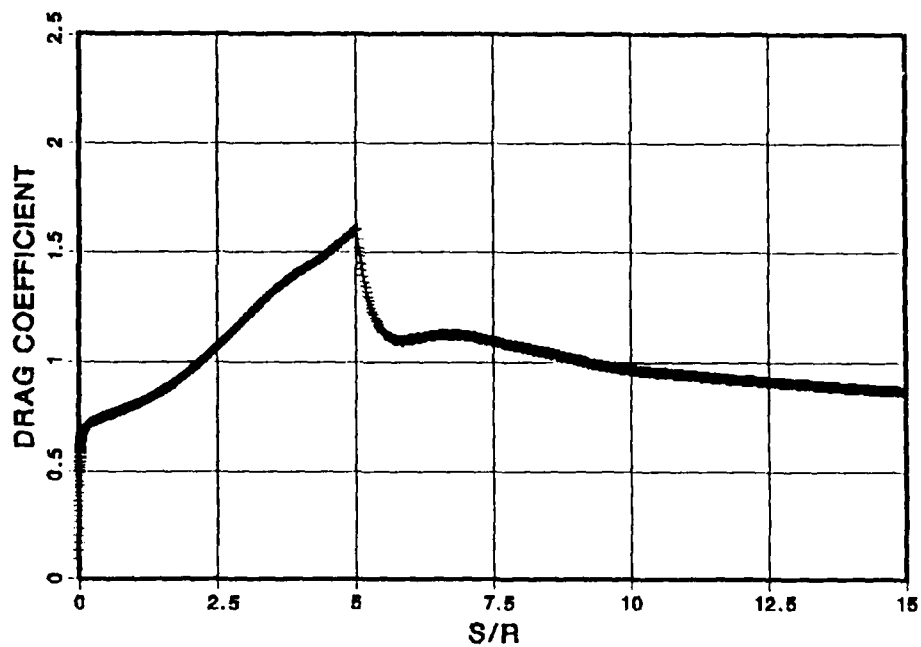
Figure 15a. C_D vs. S/R, $(S/R)_{MAX}=15$ for $(S/R)_v=5$
and No Disturbance
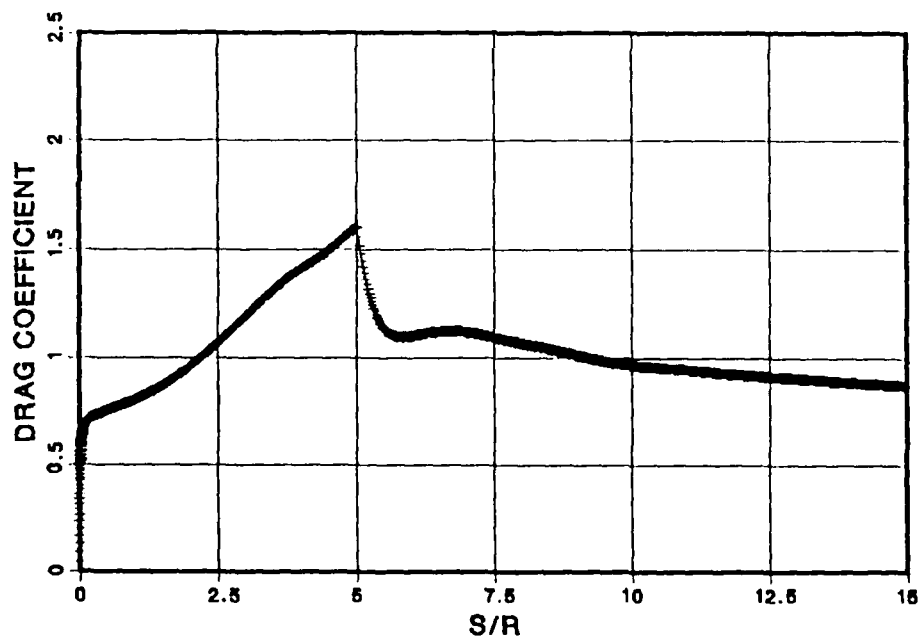
Figure 15b. C_D vs. S/R, $(S/R)_{MAX}=15$ for $(S/R)_v=5$
with $\Delta\alpha=0.5$
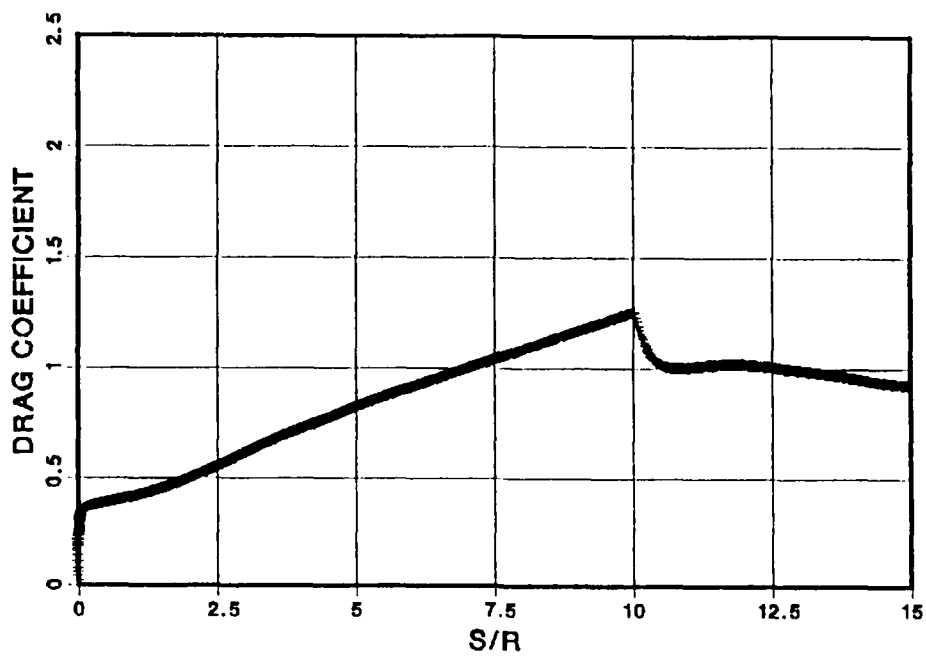
Figure 16a. C_D vs. S/R, $(S/R)_{MAX}=15$ for $(S/R)_v=10$ and No Disturbance
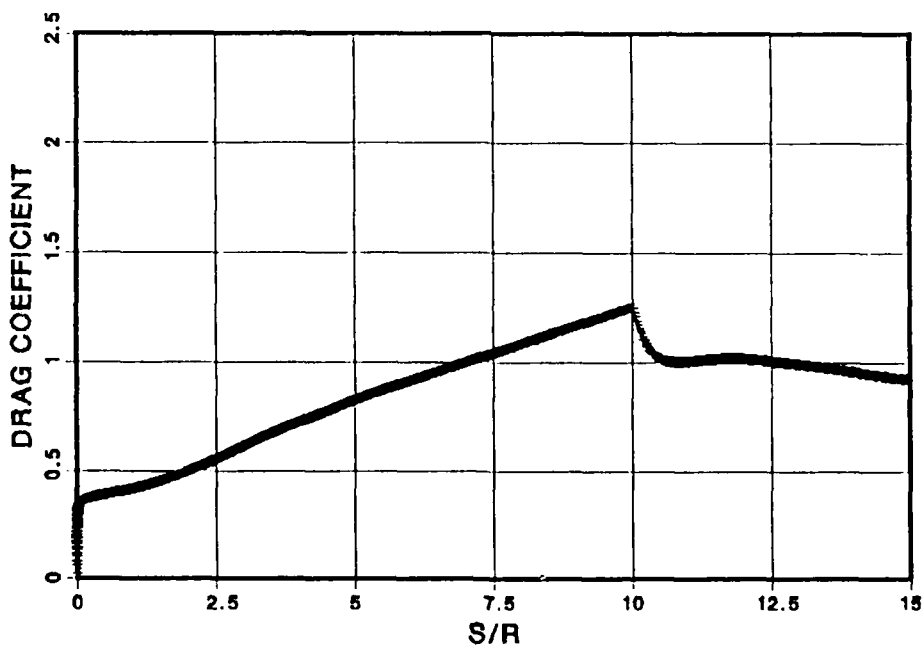
Figure 16b. C_D vs. S/R, $(S/R)MAX=15$ for $(S/R)_v=10$ with $\Delta\alpha=0.5$
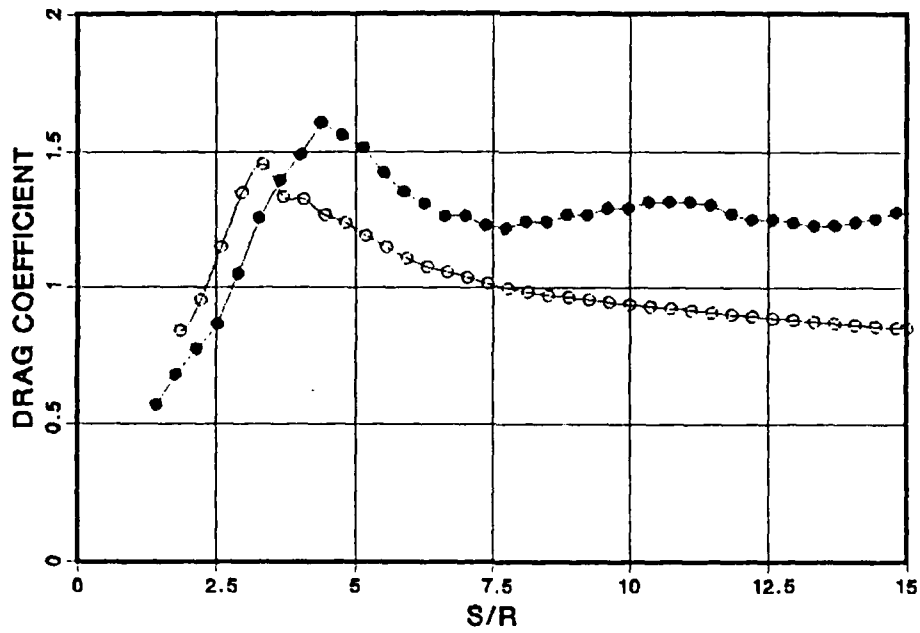
Figure 17. C_D vs. S/R for $(S/R)_v=1$, Numerical (open circles) and Experimental (full circles)
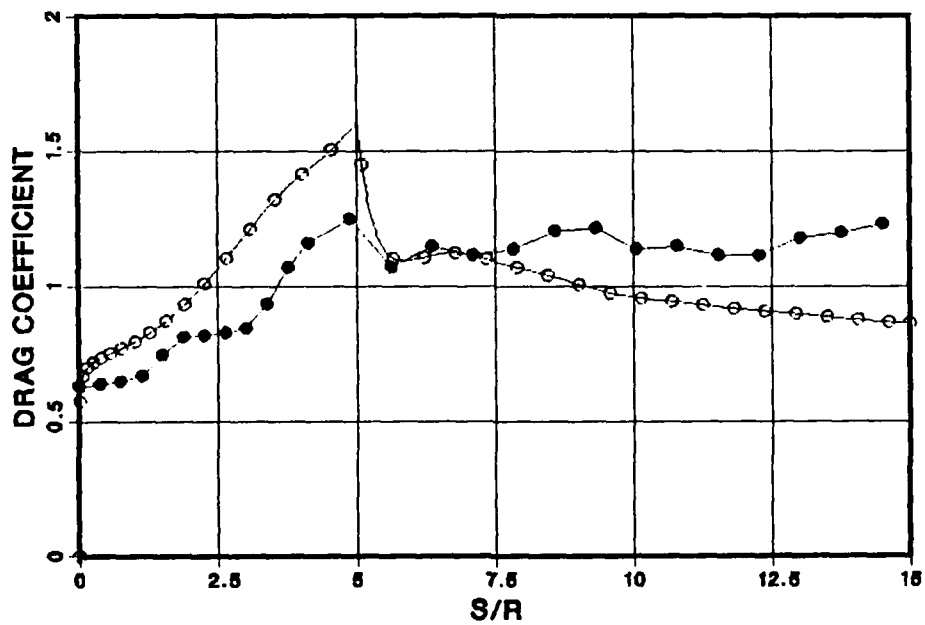
Figure 18. C_D vs. S/R for $(S/R)_v=5$, Numerical (open circles) and Experimental (full circles)
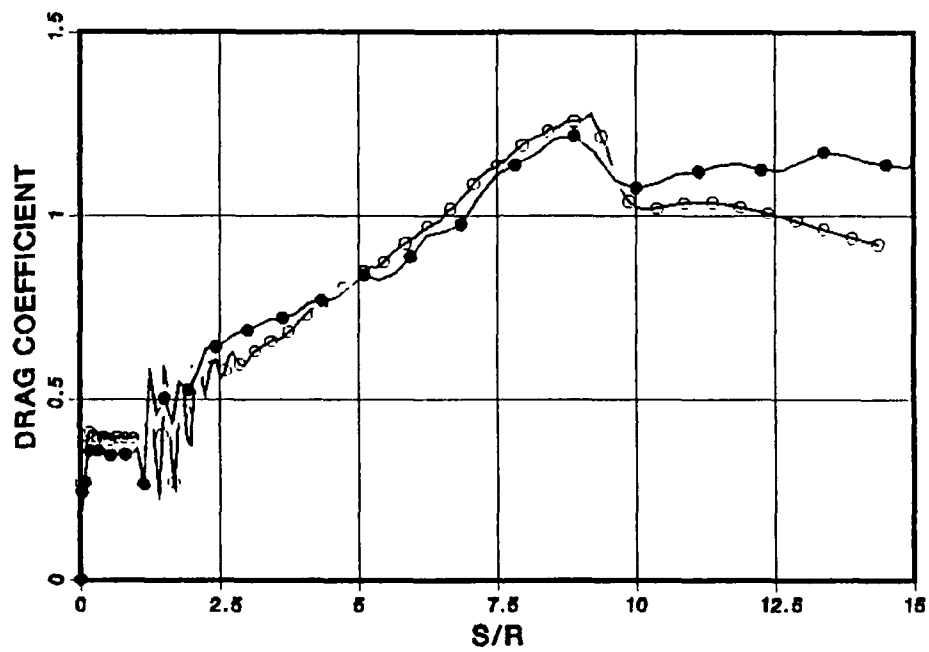
Figure 19. C_D vs. S/R for $(S/R)_v=10$, Numerical (open circles)
and Experimental (full circles)

55
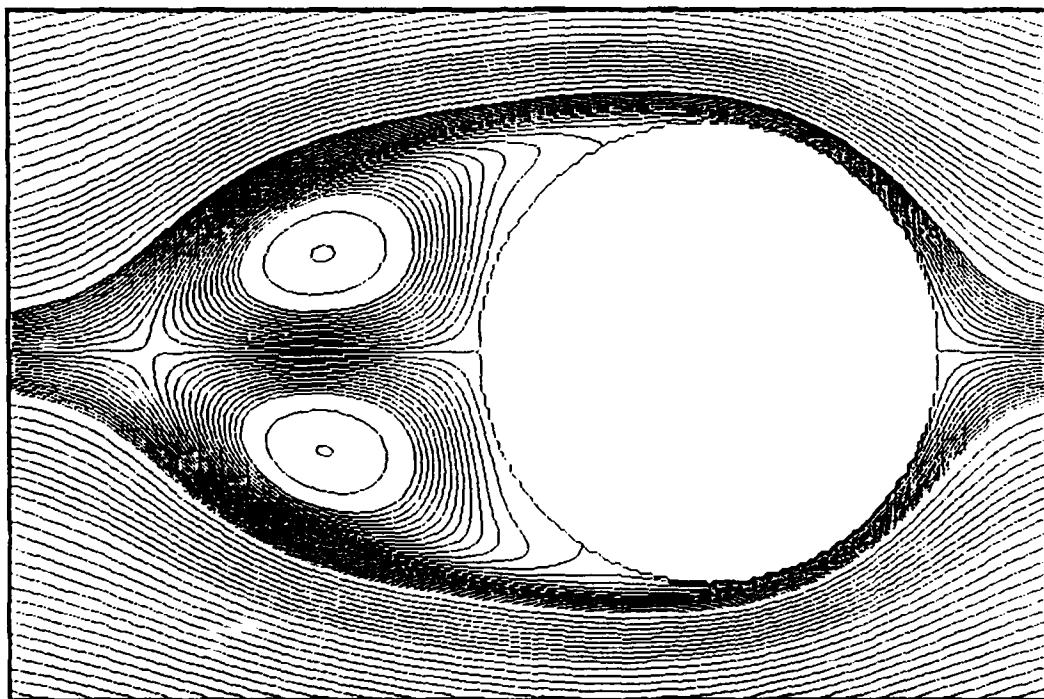
Figure 20. Streamlines at S/R=5 with No Disturbance
and $\Delta\lambda=1/64$
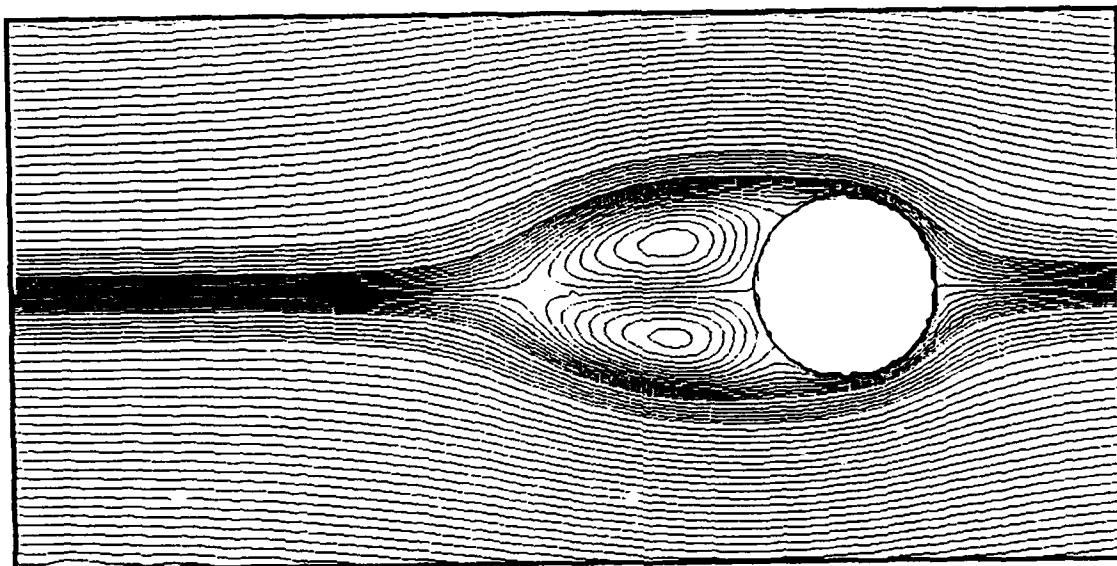
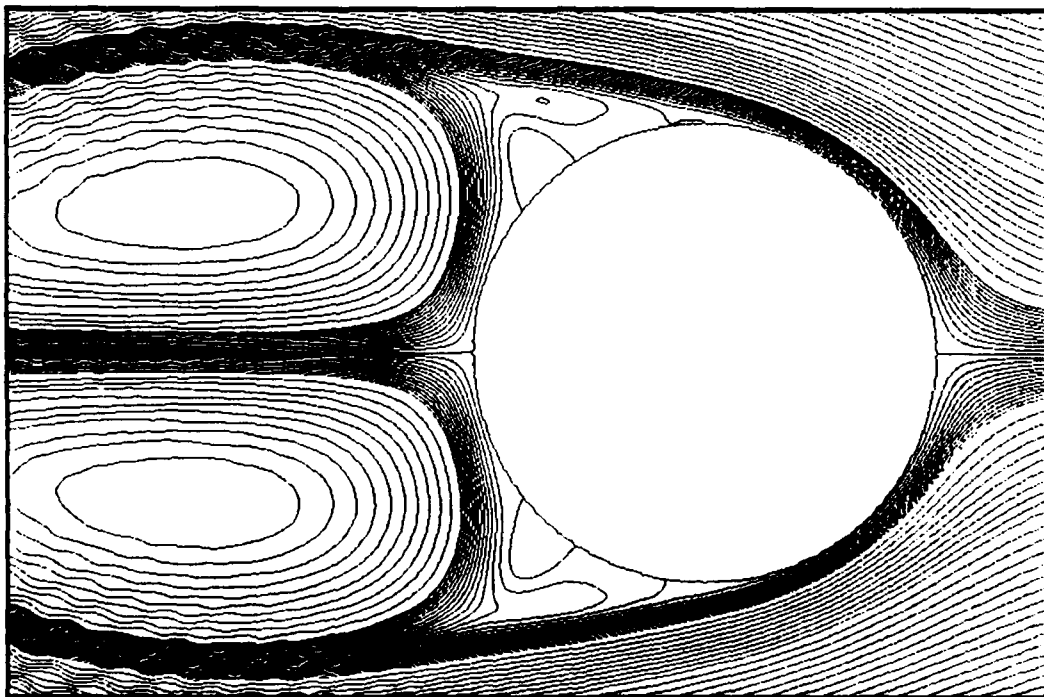Figure 21a. Streamlines at S/R=15 with No Disturbance
and $\Delta\lambda$=1/16
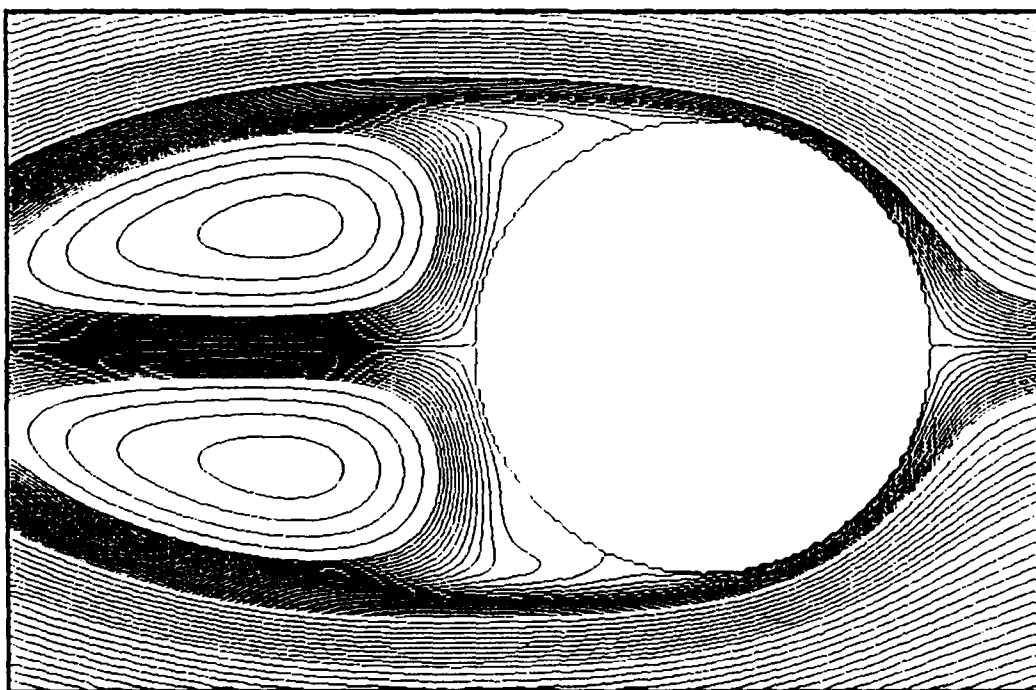
Figure 21b. Streamlines at S/R=15 with No Disturbance
and $\Delta\lambda=1/64$

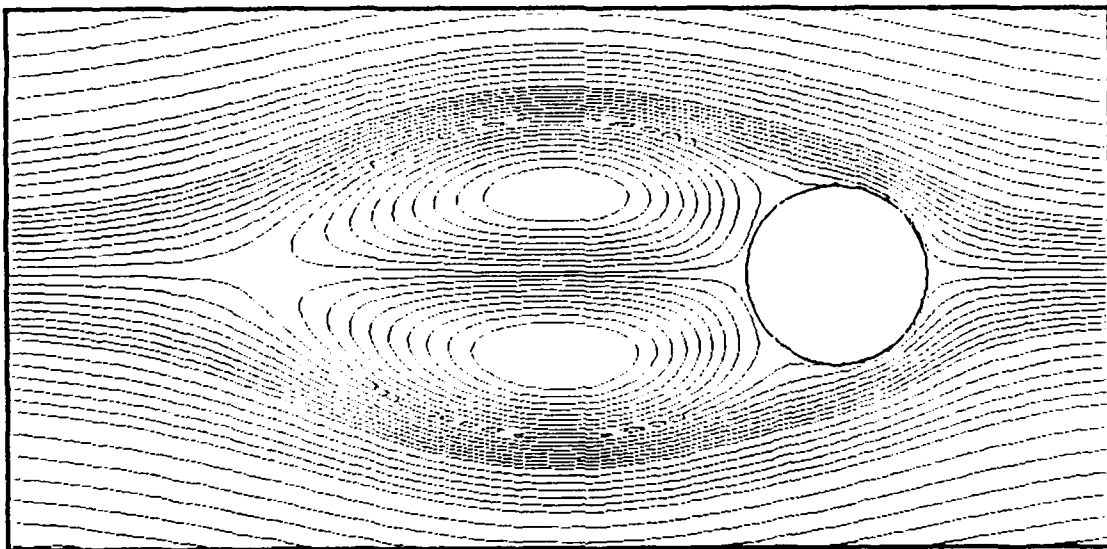Figure 21c. Streamlines at S/R=15 with No Disturbance
and $\Delta\lambda=1/160$
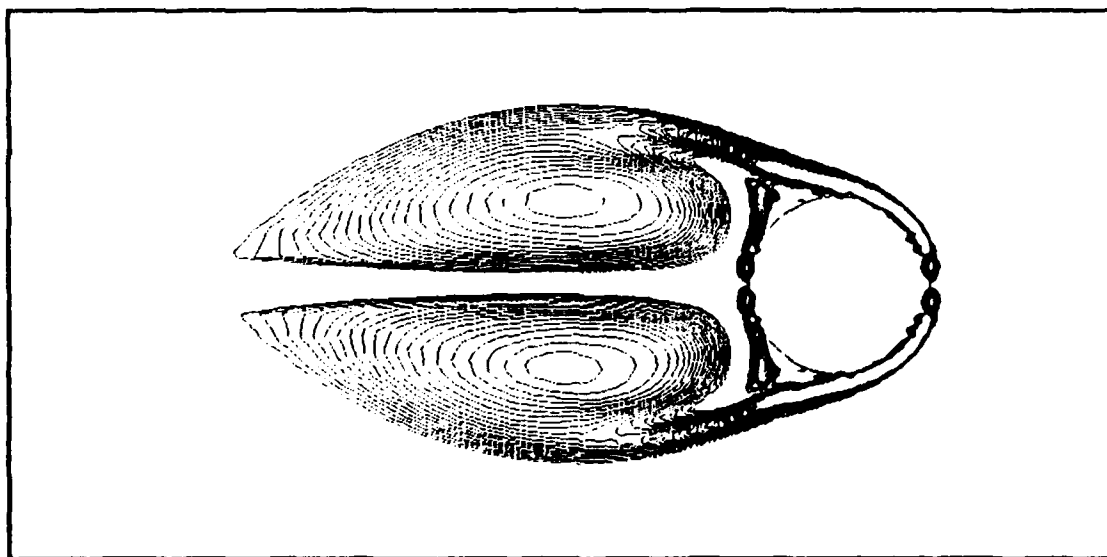
Figure 22a. Streamlines at S/R=40 with No Disturbance

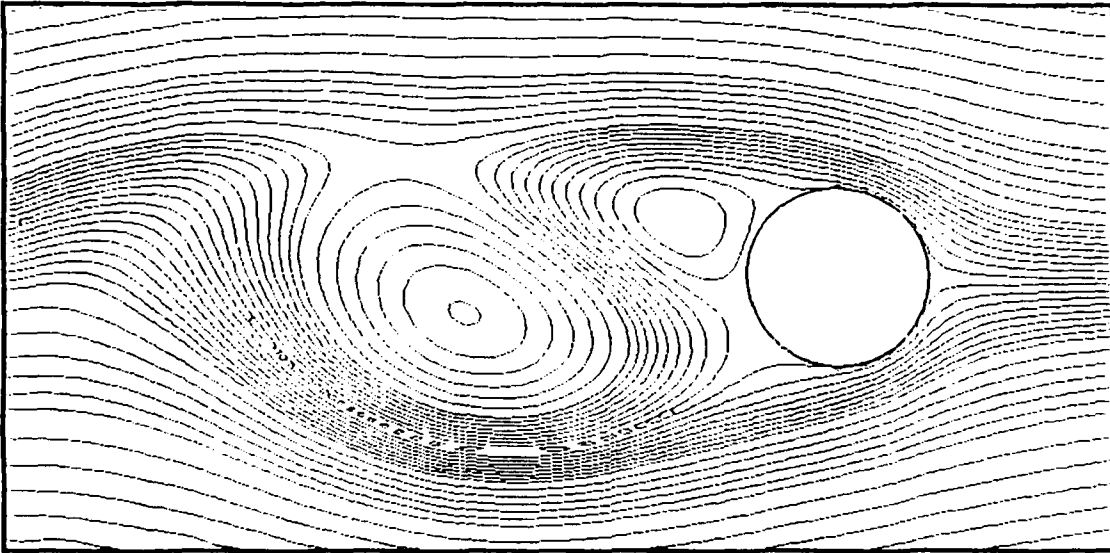Figure 22b. Vorticity Contours at S/R=40 with
No Disturbance

60

Figure 23a. Streamlines at S/R=40 with $\Delta\alpha$=0.1
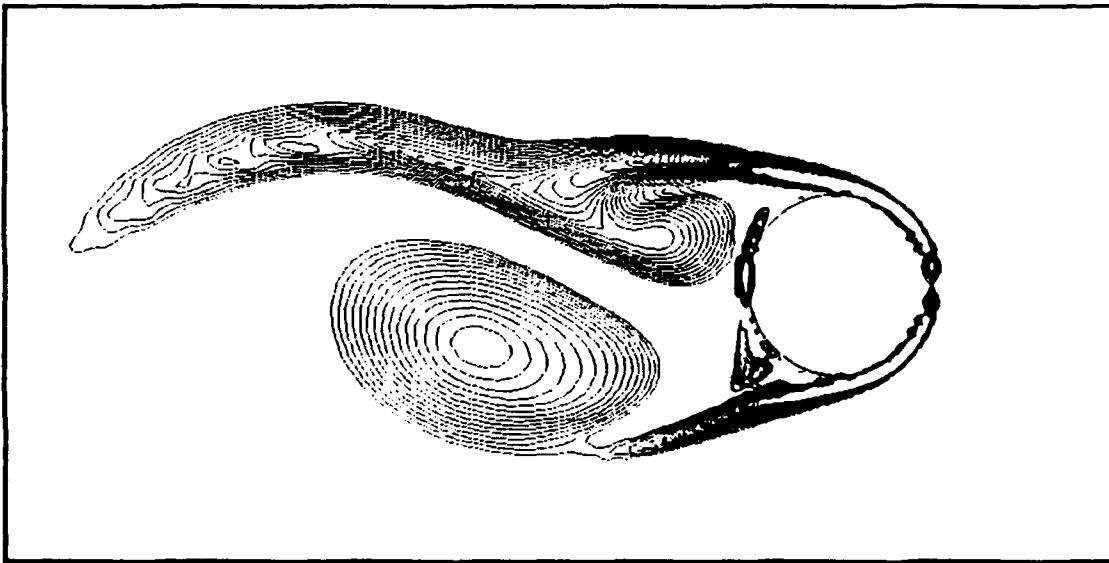

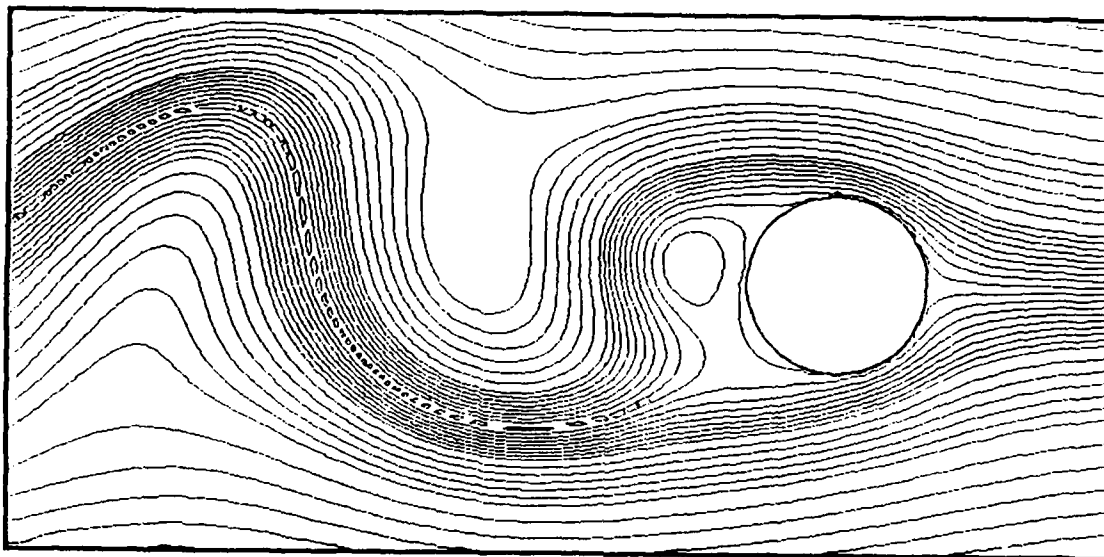Figure 23b. Vorticity Contours at S/R=40 with $\Delta\alpha$=0.1

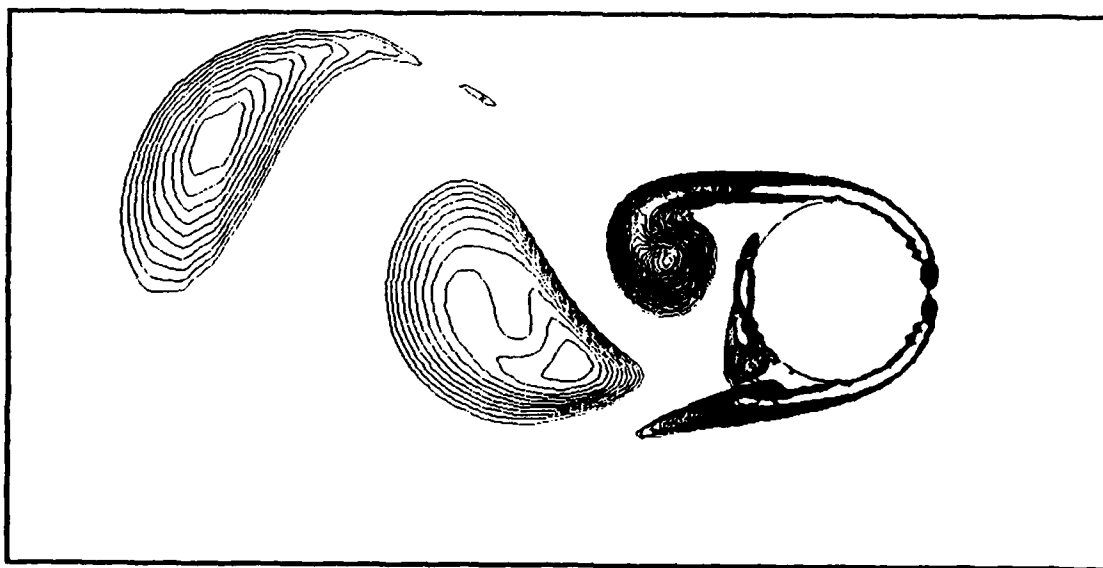Figure 24a. Streamlines at S/R=40 with $\Delta\alpha=0.5$

Figure 24b. Vorticity Contours at S/R=40 with
$\Delta\alpha=0.5$
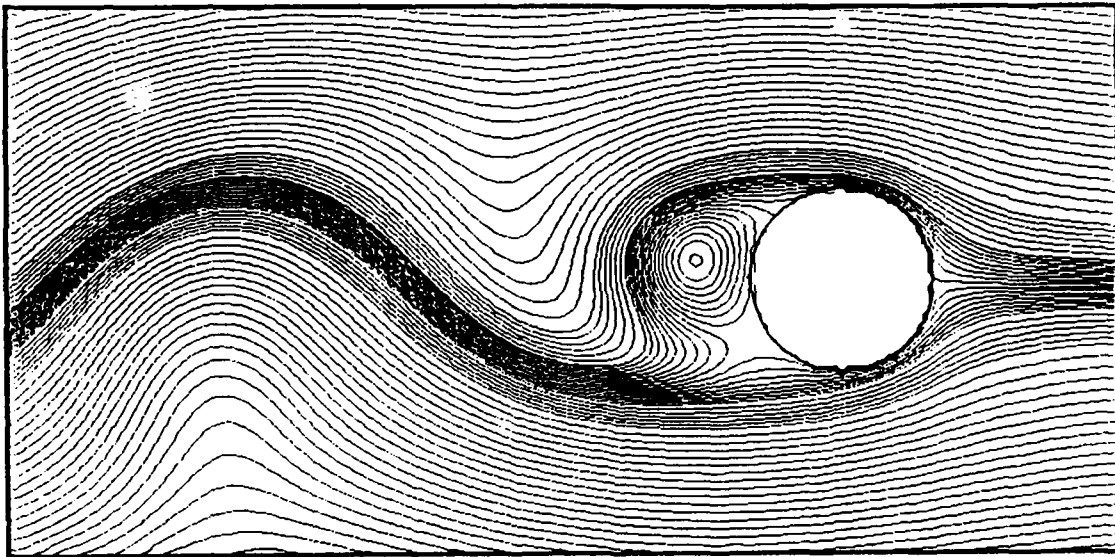
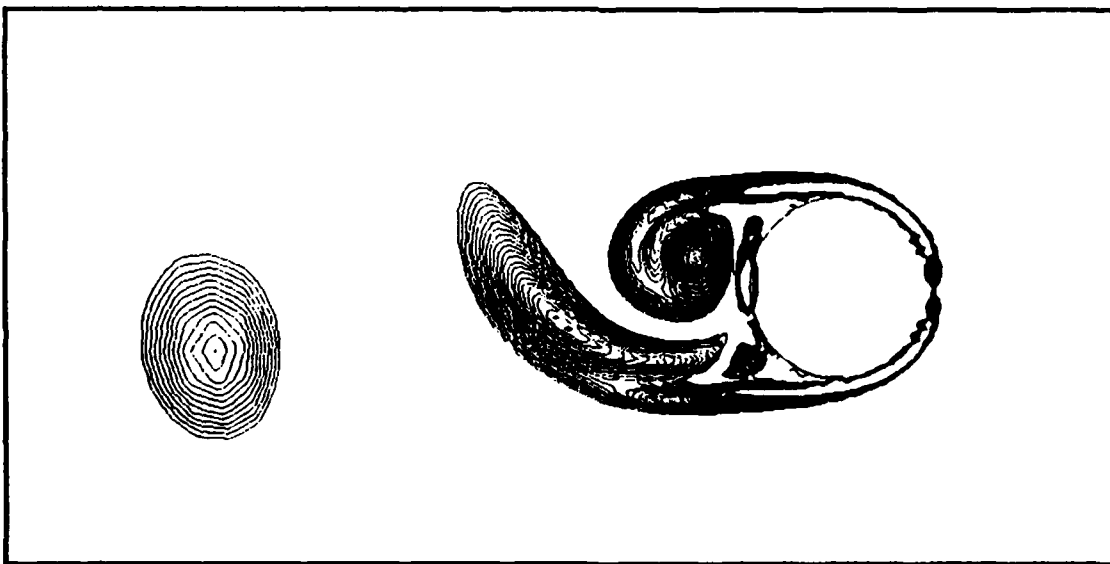Figure 25a. Streamlines at S/R=40 with $\Delta\Psi$=0.005

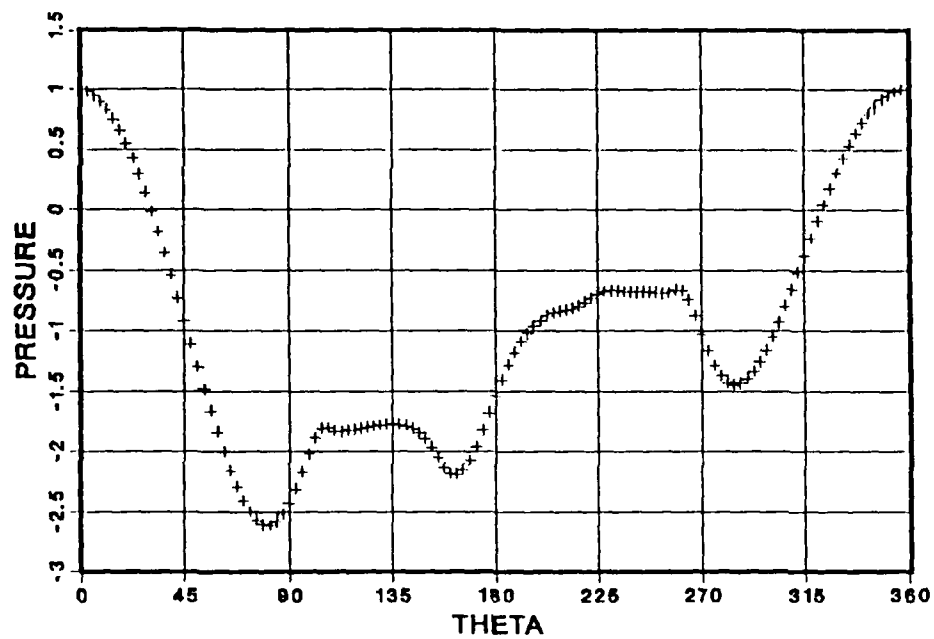Figure 25b. Vorticity Contours at S/R=40 with
$\Delta\Psi$=0.005

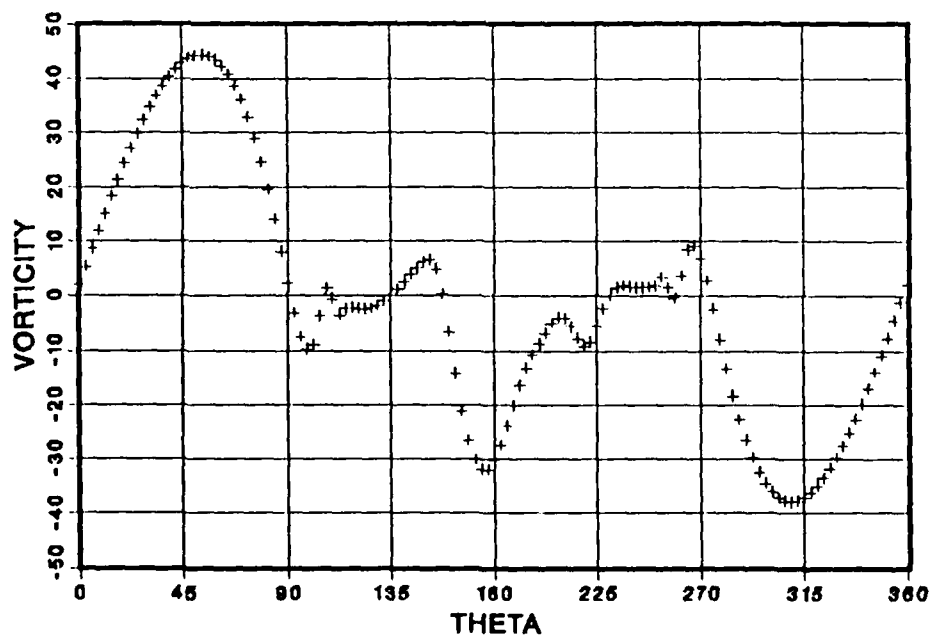Figure 25c. Pressure Distribution at S/R=40 with
$\Delta\Psi$=0.005

Figure 25d. Vorticity Distribution at S/R=40 with
$\Delta\Psi$=0.005

64

LIST OF REFERENCES

1. Ta Phuoc Loc, "Numerical Analysis of Unsteady Secondary Vortices Generated by an Impulsively Started Cylinder," *Journal of Fluid Mechanics*, Vol. 100, Part 1, pp. 111-128, 1980.

2. Lecointe, Y., and Piquet, J., "On the Use of Several Compact Methods for the Study of Unsteady Incompressible Viscous Flow Round a Circular Cylinder," *Computers & Fluids*, Vol. 12, No. 4, pp.255-280, 1984.

3. Ta Phuoc Loc and Bouard,R., "Numerical Solution of the Early Stage of the Unsteady Viscous Flow Around a Circular Cylinder; a Comparison with Experimental Visualization and Measurements," *Journal of Fluid Mechanics*, Vol. 160, pp. 93-117, 1985.

4. Chamberlain, R. R., "Unsteady Flow Phenomena in the Near Wake of a Circular Cylinder," AIAA Paper No. 87-0317, 1987.

5. Rumsey, C. L., "Details of the Computed Flowfield Over a Circular Cylinder at Reynolds Number 1200," *Journal of Fluids Engineering, Trans. ASME*, Vol. 110, pp. 446-452, 1988.

6. Sarpkaya, T., and Shoaff, R. L., "Inviscid Model of Two-Dimensional Vortex Shedding by a Circular Cylinder," *AIAA Journal*, Vol 17, No. 11, pp.1193-1200, 1979.

7. van der Vegt, J. J. W., *A Variationally Optimized Vortex Tracing Algorithm for 3-Dimensional Flows Around Solid Bodies*, Ph. D. Thesis, Maritime Research Inst., Netherlands, 1988.

8. Sarpkaya, T., "Computational Methods with Vortices-The 1988 Freeman Scholar Lecture," *Journal of Fluids Engineering, Trans. ASME*, Vol. 111, No. 1, pp. 5-52, March 1989.

9. Chang, C.-C., and Chern, R.-L., "Numerical Study of Flow Around an Impulsively Started Circular Cylinder by a Deterministic Vortex Method," (to appear in *Journal of Fluid Mechanics*), 1990.

10. Bouard, R., and Countanceau, M., "The Early Stage of Development of the Wake Behind an Impulsively Started Cylinder for $40<Re<10^4$," *Journal of Fluid Mechanics*, Vol.101, Part 3, pp. 583-607, 1980.

11. Sarpkaya T., "Separated Flow About Lifting Bodies and Impulsive Flow About Cylinders," *AIAA Journal*, Vol 3, No.3, pp. 414-420, 1966.

12. Naval Postgraduate School Technical Report No. NPS-69SL-78-008, *Impulsive Flow About a Circular Cylinder*, by T . Sarpkaya, 1978.

13. Nagata, H., Funada, H., and Matsui, T., "Unsteady Flows in the Vortex Region Behind a Circular Cylinder Started Impulsively, 2nd Report, Velocity Fields and Circulations," *Japanese Society of Mechanical Engineers*, Vol. 28, No. 245, pp. 2608-2616, 1985.

14. Sarpkaya, T., and Kline, H. K., "Impulsively-Started About Steady Flow Four Types of Bluff Body," *Journal of Fluids Engineering, Trans. ASME*, Vol. 104, pp. 207-213, 1982.

15. Sarpkaya, T. and Ihrig, C. J., "Impulsively Started Steady Flow About Rectangular Prisms: Experiments and Discrete Vortex Analysis," *Journal of Fluids Engineering, Trans. ASME*, Vol. 108, pp.47-54, 1986.

16. Wang, X., *A Numerical Study of Unsteady Flows Past A Circular Cylinder*, Ph.D. Dissertation, University of Houston, Houston, Texas, December 1989.

17. Sarpkaya T., "Non-Impulsively-Started Steady Flow About a Circular Cylinder," paper presented at the 28th Aerospace Sciences Meeting, Reno, Nevada, 8 January 1990.

18. Schlichting, H., *Boundary Layer Theory*, 7th ed., pg. 17, McGraw-Hill Book Co., 1979.